RSC Advances

This is an *Accepted Manuscript*, which has been through the Royal Society of Chemistry peer review process and has been accepted for publication.

Accepted Manuscripts are published online shortly after acceptance, before technical editing, formatting and proof reading. Using this free service, authors can make their results available to the community, in citable form, before we publish the edited article. This *Accepted Manuscript* will be replaced by the edited, formatted and paginated article as soon as this is available.

You can find more information about *Accepted Manuscripts* in the Information for Authors.

Please note that technical editing may introduce minor changes to the text and/or graphics, which may alter content. The journal's standard Terms & Conditions and the Ethical guidelines still apply. In no event shall the Royal Society of Chemistry be held responsible for any errors or omissions in this *Accepted Manuscript* or any consequences arising from the use of any information it contains.

ROYAL SOCIETY OF CHEMISTRY

www.rsc.org/advances

Solidified SNEDDS of loratadine: Formulation using hydrophilic and hydrophobic grades of Aerosil®, pharmacokinetic evaluations and *in vivo-in silico* predictions using GastroPlus™

Samridhi, Sandeep Kumar Singh*, Priya Ranjan Prasad Verma

Department of Pharmaceutical Sciences and Technology, Birla Institute of Technology, Mesra, Ranchi- 835215, Jharkhand, India

Address Correspondence

Dr. Sandeep Kumar Singh, Assistant Professor, Department of Pharmaceutical Sciences and Technology, Birla Institute of Technology, Mesra, Ranchi- 835215, Jharkhand, India

Email: dr.sandeep_pharmaceutics@yahoo.com

Phone: +91 9234653731

RSC Advances Accepted Manuscript

Abstract

In the present study, hydrophilic and hydrophobic grades of Aerosil® were employed as adsorbents to develop Solid Self-nanoemulsifying drug delivery system (S-SNEDDS) of loratadine and were evaluated for their influence on powder, physicochemical and biopharmaceutical properties. Angle of repose revealed better flowability of hydrophilic (15.61°) than hydrophobic (20.03°) S-SNEDDS. Texture analysis assessed their compaction behaviour. Low initial contact angles were formed on dry hydrophobic S-SNEDDS (19.0 °) than the dry hydrophilic one (26.7 °). Irrespective of the type of carrier, S-SNEDDS displayed more than 80% drug loading. Hydrophobic S-SNEDDS demonstrated greater drug release (59.33%) at 15 min as compared to hydrophilic S-SNEDDS (48.23%). The excipient-compatibility study indicated no possible interactions. TEM revealed non-aggregated spherical nanosized globules (<50 nm) surrounded by interfacial surfactant layer. SEM displayed spherical S-SNEDDS having uniform adsorption, and post-release effects depicted the presence of nanometric pores vacated by the previously adsorbed SNEDDS. Pharmacokinetic evaluations displayed enhanced systemic availability and plasma drug concentration attained by hydrophobic S-SNEDDS (Cmax, 185.99±18.99 ng/mL and AUC_{0-t} 425.00±17.53 ng-h/mL) than the hydrophilic S-SNEDDS (Cmax, 141.45±9.72 ng/mL and AUC_{0-t} 353.00±0.01 ng-h/mL). The in vivo-in silico assessment by the GastroPlus™ software showed good prediction accuracy with the major regional absorption from upper small intestine. The in vitro-in vivo correlation module presented the best-fit deconvolution model and correlation function for S-SNEDDS. The reconstructed absorption profile was sufficiently superimposable to the observed profiles after convolution. This study indicates great potential of S-SNEDDS towards enhancement of oral absorption of such poorly soluble

RSC Advances Accepted Manuscript

drugs and presents GastroPlus™ as a efficient tool for in vivo-in silico predictions, therefore suggesting to serve as an alternate oral delivery.

Keywords: Loratadine, Solid-SNEDDS, hydrophobic and hydrophilic Aerosil®, pharmacokinetics, GastroPlus simulation, In vitro-in vivo correlation

1.0 Introduction

Oral drug delivery systems, undeniably being the most favoured and preferred route of drug administration, still presents a major challenge for the poorly soluble drugs especially those belonging to the Class II of Biopharmaceutical Classification System (BCS). Such concern is also faced by BCS Class IV drugs which possess both solubility and permeability constraints thereby presenting even bigger challenge for formulation development. The poor aqueous solubility, low and variable bioavailability and high intra- and inter-subject variability of such drugs lead to low plasma-drug concentration, thereby rendering them unavailable at the receptor site to elicit a desired pharmacological response[1]. Amongst various formulation strategies employed for enhancement of solubility of such therapeutic agents, the application of lipids as drug carrier in Lipid-based drug delivery systems (LBDDS) is an emerging field[2-3]. The proposed mechanisms for bioavailability enhancement includes, enhanced solubilization of the drug present in molecular dispersed state, inhibition of P-glycoprotein efflux and reduced metabolism by cytochrome-P450 family of enzymes, promoting the lymphatic absorption and bypassing hepatic portal route[4-7].

With the firm entry of nanotechnology in the realm of drug delivery, constant efforts are being made to improve the therapeutic activity and to minimize undesirable side effects. One such widely accepted lipid-based nanotechnological approach is solid-self nanoemulsifying drug delivery system (S-SNEDDS) formulated from the liquid-SNEDDS, which disperse in a colloidal size range to form nanoemulsions upon aqueous dilution by

RSC Advances Accepted Manuscript

gastrointestinal fluids. These SNEDDS have been described as preconcentrates of homogenous complex systems constituting oils, surfactants and/or co-solvents which are thermodynamically stable[8-10]. S-SNEDDS combines the benefits associated with lipid-based drug delivery, nanometric size of nanoemulsion globules, SNEDDS and solid-dosage forms thereby achieving enhanced solubility, bioavailability and stability[11-14]. To overcome the problems faced by conventional liquid SNEDDS, such as stability, capsule-leakage and incompatibility issues, stringent processing requirements, S-SNEDDS are developed which incorporate liquid or semisolid ingredients into powders employing diverse solidification techniques like adsorption technique, spray drying, melt granulation, extrusion–spheronization and eutectic mixing[15-16]. Other potential advantages include (i) dosing precision offered by solid filling, (ii) ease of transfer, portability and storage, (iii) better patient compliance (specifically the geriatric patients), and (iv) diversity in solid dosage form options. Amongst various solidification techniques, the adsorption to solid carrier technique was incorporated in the present study since they offer the ease in solidification, simplicity and solvent-free processing without employing any sophisticated equipments and complex control parameters. Hydrophilic and hydrophobic grades of colloidal fumed silica (Aerosil® 200 and Aerosil® R972) were employed to prepare S-SNEDDS.

The primary objective of our present work was to develop S-SNEDDS using hydrophilic and hydrophobic solid carriers and investigate their powder flow properties, and physicochemical properties. Loratadine, a non-sedative H1-receptor antagonist (antihistaminic) was employed as the model drug owing to its low oral dose (10 mg), low and variable bioavailability (10-40%), suitable log P (4.3) and belonging to BCS class II[17,18]. Furthermore, LTD have growth-inhibitory effects on neoplastic mast cells, lowest incidence of heart rhythm disorders and cardiac deaths per million over other non-sedating

RSC Advances Accepted Manuscript

antihistaminics[19-21]. Nano-based drug delivery via S-SNEDDS may therefore augment the antineoplastic activity of the drug. A newer perspective of determining the tabletting potential of both types of S-SNEDDS was explored by investigating their compaction behaviour using Texture Analyzer-TA.XT.Plus (Stable Micro Systems, UK). The behaviour of both hydrophilic and hydrophobic S-SNEDDS when exposed to aqueous medium was explored by contact angle studies. S-SNEDDS were characterized for their solid-state properties using non-thermal (Fourier Transform Infrared Spectroscopy (FTIR) and Powder X-Ray Diffraction (PXRD)), and thermal tools (Differential Scanning Calorimetry (DSC) and Thermogravimetric analysis (TGA)) to provide rapid, versatile and reliable information about the drug-excipient compatibility. This may avoid the time consuming step of the annealing of the mixtures under long-term stress conditions[23]. Furthermore, the morphological characterization was carried out by advanced and sophisticated instrumental microscopic techniques like Scanning Electron Microscopy (SEM) and Transmission Electron Microscopy (TEM). The surface morphologies of both hydrophilic and hydrophobic S-SNEDDS before and after drug release were observed by SEM, in an attempt to study the mechanism and post-effect of release of adsorbed moieties.

The secondary objective of the present work aimed at pharmacokinetic evaluation of and in vivo-in silico assessment of the developed hydrophilic and hydrophobic LTD loaded S-SNEDDS. LTD is a weak base (pKa, 4.33) having the permeability of 7.61 x 10^{-4} cm/s and solubility of 4.59 mg/mL at pH 1.2 where it is completely ionized. It is well absorbed from the GIT and reaches peak plasma levels within 1-1.5 h[17,18,21,22]. Various formulation strategies have been explored to ferry LTD such as solid dispersions[24,25], cyclodextrin complexes[26,27], inclusion complexes[28], liquid-solid compacts[29], pellet-based tablets[30] and self-emulsifying beads[31]. Some efforts have been made by Li et al to study the pharmacokinetics of pure drug

RSC Advances Accepted Manuscript

(LTD) in rats. The Cmax and Tmax of LTD was reported at ~80.0 ng/mL and 1.0 h, respectively[32,33]. In the present work, we employed the Gastroplus™ software (version 9.0, Simulations Plus Inc., Lancaster, CA, USA) to evaluate the pharmacokinetic parameters of S-SNEDDS and also to simulate their in vivo absorption profiles in order to assess the pharmacokinetic predictions based on compound parameters, physiological conditions, in vitro evaluations and in vivo absorption. It further presents the regional absorption distribution by the developed S-SNEDDS over nine physiological compartments of the gastrointestinal tract (GIT). Additionally, the IVIVCPlus module of the software was employed to evaluate the best-fit correlation function to describe the IVIVC model using various deconvolution approaches, and also to reconstruct the predicted absorption profiles in order to establish relationship between in vitro dissolution and systemic availability.

2.0 Materials and methods

2.1 Materials

Loratadine (LTD) was provided *ex gratis* from Cipla (Mumbai, India). Capmul® MCM C8 (CMC8) was gifted from Abitec Corporation (Janesville, USA). Solutol® HS15 (SHS15) was procured from BASF (Ludwigshafen, Germany). Colloidal silicas i.e Aerosil 200 (A200) and Aerosil R972 (AR972) were received as gifts from Degussa (Hanau, Germany). All other chemicals were of analaR grade. The optimized LTD loaded liquid SNEDDS (OF) constituting 80.0 mg of CMC8 and 163.95 mg of SHS15, with 3.94 % of LTD were prepared and reported by us in our earlier publication[21]. These liquid SNEDDS were then solidified using hydrophilic (A200) and hydrophobic (AR972) grades of Aerosil, as presented in the present study.

2.2 Methods

2.2.1 Preparation of LTD-loaded S-SNEDDS

RSC Advances Accepted Manuscript

The composition of optimized LTD loaded liquid SNEDDS (OF) was established by us following optimization by design of experiment (DOE) approach constituting CMC8 as oil and SHS15 as surfactant[21]. The selection of excipients were based on phase solubility studies to obtain maximum solubility of the drug in 18 excipients viz. oils, surfactants and co-surfactants, and the existence of self-nanoemulsifying region was evaluated by phase diagram studies. Thereafter, following optimization by two-factor three-level full factorial design employing desirability function, the validated optimized formulation (OF) was prepared. The liquid SNEDDS was briefly prepared by dissolving LTD into the isotropic concoction of oil and surfactant and gently heated at 50 ºC with continuous stirring to facilitate solubilization[21]. S-SNEDDS of LTD were prepared by adsorption to solid carrier technique using highly porous colloidal silica. The liquid SNEDDS formulation was added sequentially to each adsorbent separately and thoroughly mixed in mortar and pestle. The ratios of adsorbate (SNEDDS): adsorbent (solidifying agent) were optimized using hydrophilic (A200) and hydrophobic (AR972) adsorbents to obtain non-sticky free flowing S-SNEDDS powders viz. FFSA2 and FFSAR, respectively.

2.2.2 Physicochemical characterization of LTD-loaded S-SNEDDS

2.2.2.1 Powder Properties

The S-SNEDDS (FFSA2, FFSAR) were evaluated for powder properties viz. tapped density, angle of repose, Carr's index and Hausner's ratio using standard procedures[34]. The tapped density providing the true density of the solid material is exclusive of the voids and intraparticle pores whereas the bulk density which is inclusive of these voids and pores, are primarily dependent on particle-size distribution, shape and tendency of the particles to adhere to one another[35]. The angle of repose, Carr's index and the closely related Hausner's ratio are simple, fast, and popular methods of predicting powder flow characteristics.

2.2.2.2 Texture analysis

RSC Advances Accepted Manuscript

Uniaxial compression tests were performed on the prepared S-SNEDDS to determine tabletting potential of such materials. The testing was performed on a Texture Analyzer-TA.XT.Plus (Stable Micro Systems, UK) equipped with Exponent Lite software (version 5,1,1,0 Lite). An HDP/GCR granule compaction rig was tightly secured on top of an HDP/90 heavy duty platform with flat insert, which was fixed on to the instrument. The sample was filled in the circular testing area of the compaction rig, with the excess being swiped away with a flat scale. A P/45 cylindrical probe with flat surface was used for compression of the granules. At first, the probe initially travelled with a pre-test speed of 2 mm/s until the surface of the granular powder bed was detected at 0.5 g trigger force. Thereafter, the probe was made to travel with TA settings comprising of test speed of 0.1 mm/s up to a distance of 2.5 mm (target mode) and finally relaxing back-to-start position at a post-test speed of 10 mm/s. This resulted in formation of a granular compact (Gr-Co) which was then further compacted with same TA settings to form a firm compact (F-Co). This complete cycle of formation of granular compact and firm compact was performed four times, with the firm compacts being deaggregated manually to their powder forms after each cycle. The maximum force and area under curve (AUC) indicative of hardness and energy respectively, were calculated with the help of Exponent Lite software.

2.2.2.3 Drug loading efficiency

S-SNEDDS (FFSA2 and FFSAR) were weighed (100 mg) and dissolved in 10 mL distilled methanol to evaluate loading efficiency. These were then vortexed for 10 min followed by centrifugation at 3000 rpm (Remi Equipments Pvt. Ltd., India) for 10 min. The supernatant were collected, filtered through Sartorious filter paper (8 μm), suitably diluted and analyzed at 247 nm using a UV spectrophotometer. The drug loading efficiency was determined by the following equation:

RSC Advances Accepted Manuscript

$$\text{Drug loading efficiency} = \frac{\text{Amount of drug present in known quantity of formulation}}{\text{Initial drug load}} \times 100 \quad \text{Eq. 1}$$

2.2.2.4 Reconstitution study

The reconstitution ability was observed by dispersing 100 mg of S-SNEDDS in 100 mL of Millipore water (Molsheim, France) for 1 h using cyclomixer (Cyclo, Remi Equipments Pvt. Ltd.) to disperse samples completely, followed by centrifugation at 3000 rpm for 10 min[11, 36]. The supernatant were withdrawn and analyzed for optical clarity (percent transmittance) at 400 nm using UV spectrophotometer (UV-Vis Spectrophotometer, 1800, Shimadzu, Japan). The reconstitution behaviour was evaluated for mean globule size (Z-avg), Poly Dispersity Index (PDI) and zeta potential by Dynamic Light Scattering, with a Zetasizer Nano ZS (Malvern Instruments, Worcestershire, UK) at a wavelength of 633 nm at 25 ºC. The samples were also analysed 24 h post dispersion to observe any signs of phase separation or any change in the size distribution. To check for reproducibility, the analysis was carried out in triplicate.

2.2.2.5 In vitro drug release study

S-SNEDDS equivalent to 10 mg of LTD were filled in hard gelatin capsules for the *in vitro* drug release study using USP dissolution apparatus 2. The capsules were immersed in 900 mL of 0.1 *N* HCl with the aid of sinkers. The study was performed at 50 rpm and maintained at 37±0.5 ˚C. Aliquots (5 mL) were withdrawn at timed intervals up to 120 min and replenished with equal volume of fresh media to maintain the sink condition. The experiment was performed in triplicate and all samples were analyzed by the in-house validated HPLC method [37].

2.2.2.6 Contact angle studies

The wetting behaviour of S-SNEDDS (FFSA2, FFSAR) were studied by contact angle measurements using the Optical Contact Angle tester (OCAH230, Dataphysics,

RSC Advances Accepted Manuscript

Germany) equipped with a high performance 6X zoom lens and high resolution CCD camera. Water drops (5 µL) were dispensed at the rate of 1.0 µL/s to the solidified formulations (compressed into a flat cake) using Hamilton syringe DS 500/GT (O.D: 0.52 mm, I.D: 0.26 mm, and L: 51.0 mm) attached with the equipment. A series of images were captured from video sequences for measurement of contact angles formed on the dry and pre-wetted surfaces, using the software package SCA 20 version 2. The video was taken until all the liquid was imbibed, and the total time of spreading and drainage was noted.

2.2.3 Solid-state characterization

2.2.3.1 Fourier transform infrared spectroscopy (FTIR)

An IR Prestige-21 FTIR spectrophotometer (Shimadzu, Japan) equipped with attenuated total reflectance (ATR) accessory was used to obtain the infra red spectrum of drug in the isotropic mixtures of excipients. Analysis of pure drug (LTD), CMC8, SHS15 along with their physical mixtures (1:1) and co-melts (1:1) were carried out using KBr disc to investigate for possible drug-excipient interaction, if any. Optimized liquid SNEDDS (OF), solidifying agents (A200, AR972), S-SNEDDS (FFSA2, FFSAR) were also analyzed for interactions. All the samples were dried under vacuum prior to obtaining any spectra and scanned from a frequency range of 4000–600 cm^{-1}.

2.2.3.2 Powder X-Ray diffraction studies (PXRD)

Diffraction patterns of pure drug (LTD), physical mixtures (PM1, PM2) and co-melts (CM1, CM2) of drug and excipient, solidifying agents (A200, AR972) and the S-SNEDDS (FFSA2, FFSAR) were obtained by powder X-Ray diffractometer (Bruker AXS D8 Advance, Rheinstetten, Germany) to assess their crystallinity. These were scanned over 2θ range from 10° to 40° at a rate of 2° per minute at 0.02° 2θ step size.

2.2.3.3 Differential scanning calorimetry studies (DSC)

RSC Advances Accepted Manuscript

Thermal analysis of the pure drug (LTD), individual excipients (CMC8, SHS15), physical mixtures (PM1, PM2) and co-melts (CM1, CM2) in 1:1 ratio, optimized liquid SNEDDS (OF), solidifying agents (A200, AR972), S-SNEDDS (FFSA2, FFSAR) were carried out using a differential scanning calorimeter (DSC-50, Shimadzu) under purge of dry nitrogen gas (50 cc/min). Samples were placed in aluminium pans, adequately sealed by crimping with lid and heated from ambient temperature to 200 °C at a pre-programmed heating rate of 10 °C/min.

2.2.3.4 Degradation studies (TGA-DTA)

Simultaneous thermogravimetric analysis (TGA) and differential thermal analysis (DTA) techniques were used for characterization of thermal degradation of LTD, solidifying agents (A200, AR972) and S-SNEDDS (FFSA2, FFSAR). The samples were taken in aluminium pans and heated from ambient temperature to 600 °C at a heating rate of 10 °C/min under the purge of dry nitrogen gas (50 cc/min) using DTG 60 instrument (Shimadzu, Japan). The thermal stability of the sample was assessed by studying the degradation peaks and measuring the weight loss.

2.2.4 Morphological characterization

2.2.4.1 Transmission electron microscopy (TEM)

The globule shape and size of the S-SNEDDS were investigated by TEM (Tecnai 20, 200 KV, Philips, Holland). The aqueous dispersion for analysis was obtained by dispersing the formulation (100 mg) in Millipore water (100 mL), vortexing for 15 min and filtering it through Millipore filter paper (8 µm). A drop of nanoemulsion was placed over Cu-grid coated with carbon film and negatively stained using 1% (w/v) phosphotungstic acid. The grid was air-dried at ambient temperature before loading in the microscope.

2.2.4.2 Scanning Electron Microscopy (SEM)

RSC Advances Accepted Manuscript

The surface morphologies of drug (LTD), solidifying agents (A200, AR972), S-SNEDDS before drug release (FFSA2, FFSAR) and S-SNEDDS after drug release (FFSA2-D, FFSAR-D) were examined using SEM (JEOL JSM-6390LV, Tokyo, Japan) by mounting the samples onto brass stub using the double-sided tape and vacuum coating with platinum. The samples were imaged at 20 kV and at different resolutions to have better insight of the surfaces.

2.2.5 Pharmacokinetic study

Male Sprague–Dawley rats (body weight 180–200 g) were used for animal studies. Standard laboratory conditions with proper diet and water *ad libitum* were provided to animals for 5 days prior to the study. The experimental protocol was approved by the institutional animal ethical committee (No. BIT/PH/IAEC/12/2014) of Department of Pharmaceutical Sciences and Technology, Birla Institute of Technology, Mesra, Ranchi, in accordance with National Institutes of Health Guide for Care and Use of Laboratory animals[38]. Rats were fasted overnight prior to the experiment and divided randomly into two groups, each group consisting of six rats. Group I and Group II were administered with hydrophilic S-SNEDDS (FFSA2) and hydrophobic S-SNEDDS (FFSAR), respectively, each at 10 mg/kg oral dose. Blood samples were serially collected from retro-orbital sinus at time points of predose, 0.25, 0.5, 1, 2, 3, 6, 8, 12 and 24 h after oral dosing[39]. Blood samples were collected in K3-EDTA tubes followed by centrifugation (3000 rpm, 15 min) and the respective plasma samples were stored at -20 °C until analysis. The rat plasma samples were analyzed by the in-house validated liquid chromatography–electrospray ionization mass spectrometry (LC-ESI-MS/MS) method using LTD-d5 as internal standard and solid-phase extraction technique. The chromatographic separations were achieved on Gemini NX-Reverse Phase C18 (50×4.6 mm;5 μm) column (Shimadzu, Japan) using mobile phase consisting 5mM ammonium formate buffer in water (pH 3.5±0.1 with formic acid), and

RSC Advances Accepted Manuscript

acetonitrile (20:80 v/v), at a flow rate of 0.400 mL/min and injection volume of 10 µL. An API-3000 triple quadrupole mass spectrometer (MDS Sciex®; Toronto, Canada) employing positive ion-multiple reaction monitoring (+MRM) mode was used (unpublished data).

2.2.6 Pharmacokinetic analysis

The plasma pharmacokinetic parameters were calculated by non-compartmental analysis using PKPlus™ module of Gastroplus™ software (version 9.0, Simulations Plus Inc., Lancaster, CA, USA). Peak plasma concentrations (Cmax), time to reach Cmax (Tmax) and area under the plasma concentration-time curve (AUC_{0-t}) from time zero to the last measured concentration (Clast) were obtained from the plasma concentration-time curves. The elimination rate constant (Kel) was calculated from the slope of the terminal phase of the log plasma concentration–time points. AUC from time zero extrapolated to infinity ($AUC_{0\rightarrow\infty}$) was calculated as AUC_{0-t} + Clast/ Kel. The elimination half-life ($T_{1/2}$) was calculated by 0.693/Kel. Total plasma clearance (CL) was calculated by dose/AUC. Additionally, the area under the first moment curve (AUMC) was also determined by calculating the area under the product of time and concentration vs time curve. The mean residence time (MRT) is calculated by the ratio of AUMC and AUC whereas steady-state volume of distribution (Vss) is calculated as the product of MRT and CL.

The compartmental analysis (one, two and three-compartment) was performed using PKPlus™ module of Gastroplus™ software, where the model selection was based on regression coefficient (r^2) and statistical tests like Akaike Information Criterion (AIC) and Schwartz Criterion (SC). The compartmental analysis provided additional pharmacokinetic parameters like volume of the central compartment (Vc), clearance (CL), absorption rate constant (Ka), distribution rate constant (K12, K13), redistribution rate constant (K21, K31) and elimination rate constant (K10).

2.2.7 In silico assessment–GastroPlus™ simulation

RSC Advances Accepted Manuscript

The GastroPlus™ software based on advanced compartmental absorption and transit (ACAT) model, is a physiologically based oral absorption model consisting of nine compartments representing different segments of the GIT and was used to simulate the in vivo absorption profile of the developed hydrophilic and hydrophobic LTD-loaded S-SNEDDS i.e. FFSA2 and FFSAR. The program consists of three tabs for data input i.e compound, physiology and pharmacokinetics tab. The physicochemical parameters obtained experimentally or through literature or from ADMET Predictor™ (Simulation Plus Inc.) were fed into the compound tab. The experimentally determined in vitro dissolution profiles of both S-SNEDDS were loaded in the software using the tabulated in vitro dissolution data input function. GastroPlus™ default rat fasted physiology (Opt–logD model SA/V 6.1) along with the default values for transit time for each compartment was selected in the physiology tab. Absorption scale factors (ASF), calculated from these coefficients scales the effective permeability to account for variations in surface-to-volume ratio, pH effects, influx or efflux transporter differences, differences in paracellular absorption and other absorption-rate-determining effects that differ from one compartment to another[40, 41]. The micro-constants and disposition parameters obtained from the concentration–time profiles for both S-SNEDDS (FFSA2, FFSAR) were then fed into the GastroPlus™ built-in compartmental PK model to simulate their oral absorption profiles. The predicted PK parameters i.e. Cmax, Tmax, $AUC_{0\text{-}t}$, $AUC_{0\rightarrow\infty}$, cumulative intestinal absorption (Fa) and oral bioavailability (F) were then compared with the observed experimental PK parameters obtained from the best-fit compartmental model by PKPlus™ module imported into the pharmacokinetic tab. The accuracy for prediction of pharmacokinetic parameters was evaluated by the prediction fold error (Eq. 2) and the simulated model was considered to be of high prediction accuracy if the predicted values of the major pharmacokinetic parameters fall within twofold of the observed values (Fold error, FE $\leq$ 2) [42].

RSC Advances Accepted Manuscript

$$FE = 10^{\left|\log\left(\frac{\text{Predicted}}{\text{Observed}}\right)\right|} \quad \text{Eq. 2}$$

The GI absorption of the developed LTD loaded S-SNEDDS from the nine physiological compartments of GIT were also ascertained from the GastroPlus™ simulation software in order to interpret the likely regional GI absorption and also to assess the effectiveness of the delivery system.

2.2.8 In vitro-in vivo correlation

The relationship between in vitro dissolution and in vivo absorption profiles of the LTD-loaded S-SNEDDS (FFSA2 and FFSAR) were performed using the level A correlation by IVIVCPlus module of GastroPlus™ software. This module uses deconvolution followed by convolution to carry out the predictions and to reconstruct the plasma concentration profiles. The correlation between the in vivo drug release fraction and in vitro drug release was achieved using various deconvolution models viz. GastroPlus mechanistic absorption model, Numerical deconvolution and Loo-Riegelman method (two-compartment model) and regression analysis was used to select the best-fit deconvolution model. The plasma concentration-time profile was predicted and reconstructed in the convolution tab based on the in vitro and in vivo profiles of the developed formulations.

3.0 Results and discussion

3.1 Preparation of LTD loaded S-SNEDDS

Amongst various solidification techniques reviewed through literature, adsorption to solid carrier technique using colloidal silica as adsorbent was chosen to prepare LTD loaded S-SNEDDS owing to the advantages they hold. To explore the effect of solid carrier onto the physicochemical behaviour of solidified SNEDDS, adsorption was performed with two different grades of colloidal silica i.e. hydrophilic (A200) and hydrophobic (AR972) to prepare solidified formulations designated as FFSA2 and FFSAR, respectively. In order to

RSC Advances Accepted Manuscript

attain non-sticky, non-greasy and non-aggregated free flowing powders, the ratios of adsorbate (SNEDDS): adsorbent (solidifying agent) were optimized and found to be 1:1 and 1:2 for FFSA2 and FFSAR, respectively. The adsorption of 1 part of liquid lipid formulation on 1 part of A200 was sufficient to produce fine powders whereas the same 1 part of AR972 was insufficient to adsorb 1 part of the liquid lipid formulation. This clearly indicated high adsorbing potential of A200 owing to its higher specific surface area (175-225 m^2/g) as compared to that of AR972 (90-130 m^2/g)[43, 44]. The composition of the final S-SNEDDS (FFSA2 and FFSAR) includes CMC8 (80 mg), SHS15 (163.95) and LTD (10 mg) with A200 (253.95 mg) or AR972 (507.90 mg).

3.2 Physicochemical characterization of LTD-loaded S-SNEDDS

3.2.1 Powder properties

The systems of particulate solids are said to be the most complex physical systems since no two particles are identical and the nature of momentum and energy exchange defies description except in most ideal terms[45]. The derived properties of the S-SNEDDS powder viz. densities (bulk and tapped), bulkiness and flow properties (angle of repose, hausner ratio, carr's index) determined by standard procedures are tabulated in Table 1. However, the fundamental properties of the solid formulations viz. particle size and shape were later construed from the microscopic examination by SEM. Additionally, the compression and compaction behaviour of solidified formulations were assessed to evaluate their tableting capability.

The solidified FFSA2 and FFSAR were found to be of lower bulk densities i.e. 0.40 g/cm^3 and 0.39 g/cm^3, respectively, signifying the existence of large gaps between the surfaces of the packed particles. The bulk densities are useful in the ground check for bulk uniformity during filling of capsules. Moreover, the bulkiness or the specific bulk volume for

RSC Advances Accepted Manuscript

FFSA2 and FFSAR calculated to be 2.49 and 2.54, respectively, is considered to be important parameter during packaging. The tapped densities obtained after 100 taps, for both formulations were found to be in the range of 0.5 g/cm^3 ± 2%, indicating the condition of closest packing wherein the particles of smaller dimensions sift down to get placed between the relatively larger particles (Table 1). However, the smaller difference between the bulk and tapped densities indicative of the flow of particles were expressed by the Hausner's ratio and Carr's index (Table 1). The Hausner's ratios for FFSA2 (1.24) and FFSAR (1.28) were found to be lying between 1.19-1.25 and 1.26-1.34 indicating 'fair' and 'passable' flow characters, respectively. The Carr's index for FFSA2 (19.67) and FFSAR (21.50) categorized the powders to have 'fair' and 'passable' flow characteristics as per the standard ranges[34]. However, the angle of repose (θ) formed between the horizontal surface and surface of pile is considered to be a direct and accurate reflection of the bulk and flow properties of powder. Such an angle was found to be 15.61° for FFSA2 and 20.03° for FFSAR indicating 'excellent' and 'good' powder flow, respectively. The angle of repose, which is also a measure of coefficient of friction, implied existence of sufficiently smooth and regular shaped particles. Conclusively, FFSA2 showed excellent and better flowability as compared to the good and passable flowability attained by FFSAR. However, for the purpose of tableting the S-SNEDDS, a higher excellency in flow characteristics can be achieved by additional use of glidants.

3.2.2 Compaction behaviour: Texture analysis

With oral dosage forms being still preferred by patients, the ability of the powdered formulation to be compressed and compacted was also explored which would directly relate to the tableting performance of the solid formulations. The ability of the powder to decrease in volume under pressure defines the compressibility factor whereas its ability to be compressed in tablet of a certain strength or hardness indicates the compactibility of the

RSC Advances Accepted Manuscript

powders. The compressibility factor was indicated by the Carr's index and the compaction behaviour of the powder beds were studied using Texture analyzer. The four cycles of compaction, each comprising formation of granular compact (Gr-Co) and subsequent firm compact (F-Co), are displayed by the force-displacement curves of both S-SNEDDS (FFSA2 and FFSAR) in Fig. 1. The first granular compact (Gr-Co-1) resulted in achievement of 504.38 g and 654.53 g of force with 2.628 kg.sec and 3.757 kg.sec of energy (AUC) for FFSA2 and FFSAR, respectively. The subsequent formation of first firm compacts (F-Co-1) of FFSA2 and FFSAR displayed nearly same hardness of 22.554 kg and 22.563 kg, with nearly same energy consumption indicated by the AUC values of 153.933 kg.sec and 153.252 kg.sec, respectively. However, the next consecutive cycle displayed a sudden and steep rise in the hardness of the S-SNEDDS compacts (F-Co-2) with the hydrophilic FFSA2 showing more hardness (29.99 kg) as compared to the hydrophobic FFSAR with hardness of 27.609 kg. The formation of granular compacts (Gr-Co-1 to Gr-Co-4) and firm compacts (F-Co-1 to F-Co-4) of both FFSA2 and FFSAR are represented by the formation of force-displacement curves, shown in Fig. 1(A, B). The close inspection of these curves during compaction revealed the existence of yield point in firm compacts (F-Co-1 to F-Co-4) at around 0.25 mm distance, where the curve deviated to a sudden exponential rise in the slope. This yield point achieved during compaction was found to exist at yield force equivalent to the maximum force achieved during formation of granular compacts (Gr-Co-1 to Gr-Co-4). Thus, it may be inferred that during formation of granular compacts (Gr-Co-1 to Gr-Co-4) the particles initially sift down to fill up the interparticular spaces resulting in an interlocked arrangement of particles, and thereafter when compacted further, the particles try to move past another leading to deformation of the packed bed resulting in formation of firm compacts (F-Co-1 to F-Co-4). The next consecutive two cycles resulted in insignificant changes in hardness values of FFSAR as evident from the overlapping curves (Fig. 1B). However, slight rise in the

RSC Advances Accepted Manuscript

hardness values were observed with FFSA2. This may be because of formation of stronger hydrogen bridge linkages between the primary particles of hydrophilic A200 and also with the entrapped moisture. This may be advantageous if the tablet stability is to be considered. Hence, the behaviour of the particles towards compaction process is important in pharmaceutical tableting since changes in surface properties, crystallization, milling process etc may affect the flow characteristics and compactibility significantly.

3.2.3 Drug loading efficiency and reconstitution study

Both hydrophilic FFSA2 and hydrophobic FFSAR, displayed more than 80% of the drug loading, irrespective of the carrier used (Table 1). The incomplete loading of the drug could be the result of the inevitable loss which must have been incurred during the transfer into/from the mortar or during the solidification process. Reconstitution is of utmost concern since the solidified SNEDDS must self emulsify into nanoemulsion upon aqueous dilution and agitation in the GI fluid. The low absorbance values of S-SNEDDS resulted in greater than 90% per cent transmittance by the aqueous dispersion even after 24h. Marginal difference was observed in the globule sizes of FFSA2 and FFSAR with relatively larger sizes obtained in S-SNEDDS prepared with hydrophilic carrier (A200) i.e. FFSA2 (Table 1). Insignificant increase was noted in the mean globule size after 24 h of aqueous dispersion but without any sign of drug precipitation. Also, all the samples showed mono-dispersed globules revealed by low PDI (Table 1). Additionally, slight increase in globule size of redispersed S-SNEDDS in 0.1 *N* HCl (FFSA2, 27.60 nm and FFSAR, 24.60 nm; 2h) as compared to liquid SNEDDS [21](OF, 19.16 nm; 2h) was noted. This perhaps is caused by decrease in effective surfactant concentration in aqueous phase due to adsorption to the carrier. This is supported by our earlier report where similar increase in globule size for dispersed liquid SNEDDS was obtained when the surfactant concentration was reduced[11, 21, 46]. However, the absence of

RSC Advances Accepted Manuscript

precipitation and any sign of coalescence of globules, affirmed by zeta potential values closer to ±30 mV indicated stability of nanoemulsion formed upon reconstitution of S-SNEDDS (Table 1). The reconstitution into nanometric sizes confirms the suitability of the adsorption method and conversion of liquid SNEDDS into solid-SNEDDS.

3.2.4 In vitro drug release studies

The systemic absorption of the drug primarily depends on the dissolution and release of the drug in dissolution medium. Since drug dissolution may be the rate-limiting factor for drug absorption in case of BCS Class II drugs, the *in vitro* dissolution may be relevant in prediction of the likely *in vivo* behaviour of the drug. The hydrophobic FFSAR displayed faster drug release initially (59.33%) in comparison to the hydrophilic FFSA2 (48.23%) as evident from the amount of drug released (Q_t) in 15 min (Table 1). This is probably due to the fact that such carriers have a low specific surface area which improves the dissolution rate as compared to the carriers with high specific surface area as also reported by Krupa et al., 2014[47]. On the contrary, porous carriers with high specific surface area may tend to be less dispersed in GIT with a slower rate of adsorption and drug dissolution[47]. Moreover, when dispersed in liquid, the isolated surface silanol groups imparting hydrophilic character to A200 have tendency to form hydrogen bridge linkages with each other directly or indirectly via the molecules in the liquid, resulting in formation of a temporary three-dimensional lattice structure[48]. Such structures which breaks down under mechanical stress is here perhaps broken down again due to stirring/GI motility. These structural changes possibly could be responsible for the delayed release of the adsorbed drug from the surfaces of hydrophilic S-SNEDDS (FFSA2). The dissolution efficiency (% DE) achieved by hydrophilic and hydrophobic ones were found to be 60.13% and 66.38% respectively (Table 1). The dissolution profiles of FFSA2 and FFSAR were compared based on model independent

RSC Advances Accepted Manuscript

approach using difference factor (f1) and similarity factor (f2), calculated as per the US-FDA guidelines for dissolution testing of immediate release solid oral dosage forms. The difference factor (f1) which measures the relative error between the two curves and is calculated by the percent (%) difference between the two curves at each time point, was found to be 9.66 %. The similarity factor (f2) representing the measure of similarity in percent dissolution between two curves was found to be 59.37 %. Since f1 lies within 0-15 % and f2 being greater than 50%, the sameness or equivalence of the two curves can be ensured (as per the guidelines). Despite the fact that the dissolution profiles of both S-SNEDDS are somewhat similar to each other, faster drug release was observed with hydrophobic S-SNEDDS. Additionally, it is also said that Aerosil hydrophobic silica, which contains hydrophobic surface siloxane groups offers distinct advantages over Aerosil hydrophilic silica with regard to the dispersibility due to the lesser aggregation or agglomeration[48]. Interestingly, the liquid LTD-SNEDDS which was successfully developed as reported in our previous publication (DE of 73.84% in 120 min)[21], when formulated into S-SNEDDS produced more sustained effect but still achieved DE of 60.13% and 66.38% by FFSA2 and FFSAR, respectively. Such observation of slower dissolution from solidified-SNEDDS has also been reported by other authors [49, 50]. It can thus be hypothesized that liquid-SNEDDS when adsorbed onto adsorbents would be retained within the pores of the carriers either partially, or completely fill the intraparticular pores, or adsorbed as thin film on the adsorbent surface in case of carriers with low surface area. Such hypothesis is based on the occurrence of lag phase by S-SNEDDS where 65% of LTD is released in 58.78 min and 45.18 min from FFSA2 and FFSAR, respectively, in contrast to liquid LTD-SNEDDS releasing the drug in mere 4.79 min [21]. It is during this lag phase that the SNEDDS is embedded within the carrier and entrapped in the intraparticular pores, and the duration is primarily depends on the adsorbing capacity, size, and specific surface area of the adsorbent. The drug dissolution and

RSC Advances Accepted Manuscript

release is therefore dependent on the physical retention of the lipid formulation in the intraparticular pores and the area of contact, which are themselves dependent on specific surface area and particle size of the adsorbent. The type of retention as previously hypothesized, would determine the total contact area which acts as nucleation sites for the drug present in liquid-SNEDDS. Larger area of contact would lead to greater nucleation rate and thus may result in precipitation of the drug, as stated by Agarwal et al., 2009 [49]. Formulations like FFSA2 having relatively larger specific surface area (175-225 m^2/g) than FFSAR (90-130 m^2/g) would provide greater area of contact leading to a greater potential for nucleation which decreases the extent of drug release. The impact of contact area on nucleation is based on the fact that the surface silanol groups on FFSA2, a potential proton donor as well as acceptor, would significantly affect drug affinity to its surface specifically the hydrophobic molecules like LTD by formation of low energy van der Waal and London forces [50, 51].

3.2.5 Contact angle studies

Wettability study indicates the degree of wetting of a solid when in contact with liquid and involves the measurement of contact angle as the primary data. The liquid penetration into both dry and pre-wetted surfaces of S-SNEDDS was studied by measurement of contact angle and the total drainage time. The contact angles which the liquid forms on the dry and pre-wetted surfaces of FFSA2 and FFSAR over the due course of liquid penetration are shown in Fig. 2. Since the granules of S-SNEDDS are prepared by porous carriers (A200 and AR972), the compressed powder cakes having inherent porous structure resulted in spontaneous penetration of the liquid drop. Though the penetration was spontaneous, the difference in contact angles and total drainage time taken by the dry and prewetted hydrophilic and hydrophobic S-SNEDDS were quite explicit. The visual differences in

RSC Advances Accepted Manuscript

contact angles amongst FFSA2-dry, FFSA2-wet, FFASR-dry and FFSAR-wet are shown in Figure 2 at common time points of 0, 2.7 and 8.4 sec. The FFSA2-dry and FFSAR-dry resulted in initial contact angles (0 sec) of 26.7 ° and 19.0 °, respectively, with total drainage time of 8.75 sec and 10.07 sec. The probable reason for larger initial contact angle formed on hydrophilic FFSA2 is the high porosity of the A200 carrier as compared to AR972. This is said so, due to the established fact that porous compressed powders tend to have larger contact angle than its counterpart, as reported by Yuan and Lee [52]. However, the undoubtedly longer drainage time taken by FFSAR-dry is due to the hydrophobic nature of its carrier leading to restricted motion of liquid as it advances into the bed. These effects were more prominent when the contact angles were measured on pre-wetted powders. The presence of moisture on the pre-wetted surface of FFSA2 (FFSA2-wet) enhanced the wettability of the surface as evident by lower contact angle of 26.0 ° (0 sec). The drop spreads readily with low drainage time of 7.75 sec due to the reduced friction by the presence of liquid on the top layer of surface as well as in the pores. The initial contact angle (0 sec) formed on the surface of pre-wetted FFSAR (FFSAR-wet) was found to be higher (24.3°) than that formed on FFSAR-dry (19.0°). Moreover, the total drainage time attained by FFSAR-wet was found to be quite high i.e. 23.85 sec, perhaps owing to hydrophobicity. In spite of the differences, the contact angles were still lower than 90 ° which reveals good wettability of both the S-SNEDDS. The good wettability is plausibly due to the reduced interfacial tension between the solid particles and the liquid, provided by the non-ionic surfactant present in the SNEDDS, which is adsorbed to these solid carriers. This might be advantageous to keep the particles dispersed in the aqueous medium. The observed phenomenon of wetting would provide a direct insight into the behaviour of S-SNEDDS when exposed to aqueous medium or its behaviour towards presence of moisture during lubrication and tabletting.

RSC Advances Accepted Manuscript

3.3 Solid-state characterization

3.3.1 Fourier transform infrared spectroscopy (FTIR)

The interaction between the drug and the excipients often leads to identifiable change in the infrared profile of the pure drug. IR spectra of loratadine (LTD), individual excipients (CMC8 and SHS15) and physical mixtures (PM) and co-melts (CM) of the drug with individual excipients are given in Supplementary Fig. S1A. LTD showed characteristic absorptions at 1701 cm^{-1}(C=O ester stretch); 1222 cm^{-1} (C–O stretch); 1643 cm^{-1} (C=N stretch); 2985 cm^{-1} (=CH stretch); 1566 cm^{-1} and 1469 cm^{-1} (benzene ring stretch) [53]. The spectral data showed the retention of the characteristic absorption of LTD in1:1 physical mixtures (PMs) and co-melts (CMs) with each individual excipient, indicating retention of chemical identity of loratadine. However, slight reduction in peak intensities and broadening of the peaks were observed in the PMs and CMs, possibly due to the mixing or the loss of crystallinity. The FTIR of optimized liquid SNEDDS (OF), the solidifying agents (A200 and AR972) and the respective solid-SNEDDS (FFSA2 and FFSAR) are shown in Supplementary Fig. S1B. The characteristic peaks of LTD were found to be retained but slightly broadened in OF, FFSA2 and FFSAR. Thus, the FTIR spectral data confirms that all the excipients does not alter the performance characteristic of the drug, indicating their compatibility.

3.3.2 Powder X-Ray diffraction studies (PXRD)

The high temperatures achieved by thermal analysis could result in potential drug/excipient degradation, which may significantly influence the performance characteristics of the drug and formulation. To overcome this limitation, PXRD analysis was also conducted. Crystallinity of the particles, determined through powder PXRD is important quality attribute to identify changes in polymorphism, stability, solubility and dissolution rate etc. X-ray diffractogram confirmed the crystallinity of LTD, with sharp and distinctive peaks

RSC Advances Accepted Manuscript

at 2θ angles of 15.106, 16.253, 16.471, 19.482, 21.056, 22.823, 23.548, 23.787 and 30.424 (Fig. 3A). All the major characteristic crystalline peaks for LTD were retained in the physical mixtures and co-melts of the drug and excipients, though at reduced intensities (Fig. 3A). The adsorbents (A200, AR972) showed no intrinsic peaks (Fig. 3B). PXRD analysis which demonstrated diffused spectra of S-SNEDDS, without any characteristic peaks of LTD owing to amorphization of LTD during formulation (Fig. 3B). Thus, in addition to the advantages of self-emulsifying formulations, amorphization of the drug is expected to show better dissolution behavior owing to nanometric sizes and absence of crystallinity. The study also indicates absence of any sign of precipitation of LTD when formulated into S-SNEDDS. This was also supported by SEM images wherein no drug precipitation or crystallization was observed on the surface of S-SNEDDS.

3.3.3 Differential scanning calorimetry studies (DSC)

Thermal analysis of the drug (LTD), pure excipients (CMC8, SHS15), solidifying agents (A200, AR972) physical mixtures (PM1, PM2) and co-melts (CM1, CM2), optimized liquid SNEDDS (OF), solidifying agents (A200, AR) and S-SNEDDS (FFSA2, FFSAR) are presented in Fig. 4. DSC monitors the endothermic and/or exothermic peaks in a system, occurring as a result of heat gained and/or lost due to changes within the sample as a function of temperature. A sharp endothermic peak of LTD at 134.61 ºC corresponding to the melting point of the drug indicates its crystalline nature. No distinct endothermic peak was observed in pure excipients (CMC8, SHS 15, A200, AR972). The PMs and CMs showed absence of LTD peak suggesting complete solubility of LTD in the excipients indicating good solubility. No new endothermic and exothermic peaks were observed in the PMs and CMs, indicating no incompatibilities. The optimized liquid SNEDDS formulation (OF) revealed an endothermic broadening in the range of 125-135 ºC. So, it is probable that during DSC measurement the solid drug (when present) dissolves in the molten carrier and is no more

RSC Advances Accepted Manuscript

present in its undissolved form in the system, when the melting temperature of LTD is reached. Moreover, the solidifying agents too did not display any endothermic peak over the entire range tested. However, slight exothermic behaviour was observed in the solidifying agents and S-SNEDD formulations, in the range of 70-80 ºC but with absence of any thermal degradation being observed as explicit from the DTA/TGA curves. As shown in Fig. 4B, the S-SNEDDS (FFSA2 and FFSAR) did not show any definite melting endothermic peak due to molecular dispersion of the drug in the lipidic excipients, which was also supported by PXRD analysis where diffused spectra of S-SNEDDS indicated amorphization of the drug. Conclusively, the physical nature of LTD converted from erstwhile crystalline state to the amorphous state may be stated when formulated in SNEDDS and S-SNEDDS.

3.3.4 Degradation studies (TGA-DTA)

DSC in conjunction with DTA analysis provides a complete picture of endothermic and/or exothermic peak(s) since either alone does not provide conclusive results about the thermally induced incompatibilities [54]. Additionally, change in the thermal event is measured by the change in mass of sample as a function of controlled temperature, obtained by TGA curves. The endothermic peak of LTD at 134.61 °C corresponding to the melting point of the drug in atmospheric nitrogen obtained from its DTA curve (Fig. 5A) was found to be in agreement with the DSC results. However, a broader endothermic peak of LTD observed at 305.73 °C (DTA/TGA curves) indicated the evaporation of the drug sample. The thermogravimetric analysis (TGA) confirmed the thermal stability of LTD up to 200 °C. However, a single stage thermal decomposition led to nearly 100% (98.55%) weight loss between 200 and 400 °C (LTD, Fig. 5B), consistent with the results reported by Ramos and Cavalheiro, 2007 [55]. The solidifying agents, A200 and AR972 reported absence of any endothermic and/or exothermic peaks in the DTA curves (Fig. 5A). Smooth decline in the

RSC Advances Accepted Manuscript

TGA curves of the solidifying agents, A200 and AR972 was observed up to 600 ℃ with a total weight loss of 16.11% and 15.41% respectively (Fig. 5B). This insignificant loss of mass is probably the result of desorption/drying. The thermal analyses of solid-SNEDDS (FFSA2 and FFSAR) presented a multi-stage (two-stage) slow decomposition over the temperature range of 200-400 °C without formation of any intermediates, evident from the smooth decline of the curves. The first stage decomposition occurred in the range of 170-320 °C with weight loss of 22.23% in FFSA2 and 15.81% in FFSAR as evident from the TGA curves of S-SNEDDS (Fig. 5B). However, the second stage decomposition in the range of 320-405 °C was showed a steeper decline in the TGA curves with a weight loss of 26.95% in FFSA2 and 20.62% in FFSAR (Fig. 5B*).* A relatively greater weight loss was observed with FFSA2 probably due to splitting off of silanol groups present on the surface of its hydrophilic carrier (A200) due to the thermal treatment. The DTA curves of FFSA2 and FFSAR presented in Fig. 5A showed absence of any endothermic/exothermic peak in the region of melting point of the drug, thereby confirming the amorphous state of LTD when formulated in S-SNEDDS. The presumption of amorphization was well supported by the results of DSC and PXRD. However, a slight shift in the broader endothermic peak of LTD in FFSA2 (376.44 °C) and in FFSAR (372.80 ℃) (Fig. 5B), clearly indicates that the evaporation of LTD was shifted to higher temperatures resulting in better thermal stability when formulated in S-SNEDDS. Conclusively, the thermoanalytical curves of S-SNEDDS and their components did not report presence of any additional peak or drastic weight loss, thereby ruling out any sign of thermally induced incompatibilities over the temperature ranges mentioned.

3.4 Morphological characterization

3.4.1 Transmission electron microscopy (TEM)

RSC Advances Accepted Manuscript

TEM images of S-SNEDDS (FFSA2, FFSAR) post aqueous dilution in Millipore water are shown in Fig. 6. It could be seen that spherical nanoemulsions were formed with no signs of coalescence. Furthermore, no signs of drug precipitation were observed inferring the stability of formed nanoemulsions. Large proportion of the globules were found to be in the size range less than 50 nm in the S-SNEDDS prepared by both hydrophilic and hydrophobic carrier. However, the sizes of nanoemulsion globules of FFSAR (Fig. 6B) were observed to be slightly smaller than those of FFSA2 (Fig. 6A). Closer analysis of TEM image in Fig. 6C reveals that each globule is surrounded by a thick layer which can be hypothesized to be that of the surfactant (SHS15). This layer provides a mechanical barrier to prevent the coalescence of formed nanoemulsions and precipitation of drug, thereby providing stability to the dispersed system. This hypothesis was well established by us earlier [56]. Moreover, the nanometric sizes of the nanoemulsion globules were consistent with the results obtained by the DLS.

3.4.2 Scanning electron microscopy (SEM)

The surface morphology of the pure LTD appeared to be crystalline in nature, clearly visible at magnifications of x2500 and x5000 (Fig. 7A and 7B). The surface morphologies of solidifying agents viz. A200 and AR972 (x2500) appeared to be amorphous, smooth and porous surface (Fig. 7C and 7D). In contrast to the presence of mesopores on the surface of A200, the surface of formulation FFSA2 particles appear to be smooth due to the fact that the pores on the surface is completely filled with liquid SNEDDS (Fig. 7E). The formulations prepared from AR972 (FFSAR) appeared to have relatively rough surfaced particles as compared to that of FFSA2. This is perhaps due to the low specific area of AR972 where the pores are overfilled by the liquid lipid formulation and the liquid is adsorbed on the external surface of the particles. Such possibilities of adsorption of SNEDDS on the surface of adsorbents have been diagrammatically explained earlier by Agarwal et al., 2009 [49].

RSC Advances Accepted Manuscript

However, both S-SNEDDS (FFSA2 and FFSAR) appeared to have nearly spherical shape, indicating that the liquid SNEDDS containing amorphous LTD are either adsorbed, coated on the surface or inside the pores of the adsorbent[11, 57]. Furthermore, the post-effect of drug release on surface morphology was observed in a manner established by us previously[11]. The SEM images of FFSA2 and FFSAR before release and the dried residues of the same (FFSA2-D and FFSAR-D) obtained after drug release are displayed at x5,000 magnification in Fig. 7 (G-J). The images revealed the existence of particles with numerous pores, undeniably different from any of the SEM images of LTD, A200, AR972, FFSA2 or FFSAR. A closer look into these pores (x5,000) reveals presence of larger pores on the dried residues of FFSA2 (FFSA2-D) in comparison to those of FFSAR-D, apparently due to larger porosity of A200. These images thus present a clear picture of the probable release of SNEDDS from these pores, which were initially adsorbed on these carriers. Moreover, the absence of crystalline LTD particles on the surface of S-SNEDDS supports the results of DSC and PXRD confirming the presence of amorphous state of the drug as dried emulsion on the surface of solidifying agent. Furthermore, the unaltered performance characteristic of LTD in terms of non-recystallization in S-SNEDDS, affirms the efficiency of the adopted solidification technique.

3.5 Pharmacokinetic analysis

The pharmacokinetic analysis was performed by the validated LC-MS/MS method after oral administration of LTD loaded S-SNEDDS. The mean concentration–time profile of the hydrophilic and hydrophobic S-SNEDDS i.e FFSA2 and FFSAR are presented in Fig. 8. The PK parameters calculated by non-compartmental and compartmental analysis using PKPlus™ module of Gastroplus™ software is tabulated in Table 2. The compartmental analysis performed to obtain a visual representation of rate processes and micro-constants involved in drug disposition, showed the best-fit 2 compartment modelling for FFSA2 and

RSC Advances Accepted Manuscript

FFSAR based on low AIC and SC values with high R^2 values (Table 2). Significant differences in some PK parameters like MRT, $T_{1/2}$ and CL were observed between different compartmental models since they possess central and multiple peripheral hypothetical compartments where body is not considered homogenous and that the distribution is not instantaneous. The non-compartmental analysis revealed that FFSA2 and FFSAR presented mean area under the curve (AUC_{0-t}) of 353.00±0.01 ng-h/mL and 425.00±17.53 ng-h/mL, respectively, with the mean Cmax values of 141.45±9.72 ng/mL and 185.99±18.99 ng/mL, respectively. The PK parameters of liquid LTD-SNEDDS and LTD-suspension established by us previously displayed an AUC_{0-t} value of 633.00±12.44 ng-h/mL and 287.00±9.11 ng-h/mL, respectively, with the mean Cmax values of 466.65±18.94 ng/mL and 104.75±2.87 ng/mL, respectively (Unpublished data). Thus, in the present work, the developed LTD loaded S-SNEDDS i.e FFSA2 and FFSAR explicitly demonstrates a 1.23-fold and 1.48-fold enhancement of oral absorption, respectively, with and 1.35-fold and 1.78-fold increase in maximum drug concentration, as compared to the LTD suspension. However, the developed S-SNEDDS shows lower AUC_{0-t} and Cmax values than the liquid SNEDDS. The outcomes of in vivo studies are consistent with the in vitro drug release studies where the order of LTD release and plasma drug concentration is FFSAR > FFSA2. Such in vivo and in vitro observations have also been reported earlier with exploration of SNEDDS potential [46, 50]. The low in vitro cumulative drug release and low in vivo plasma concentration of S-SNEDDS is likely caused by the incomplete desorption indicated by incomplete recovery of LTD in aqueous medium as compared to its liquid-SNEDDS form. The in vitro data suggesting reduced ability of FFSA2 compared to FFSAR to present LTD in solubilized state (Table 1), were also reflected in the in vivo studies (Table 3). Lower values of AUC and Cmax were achieved when formulated using hydrophilic A200 (FFSA2) as compared to that formulated using hydrophobic AR972 (FFSAR). The plausible explanation for such an effect have been

RSC Advances Accepted Manuscript

previously explained in the in vitro studies, where the presence of isolated silanol groups on the surface of A200 tends to form hydrogen bridge linkages, and/or low energy van der Waal and London forces which facilitate nucleation and entrapment of drug in the intraparticular pores thereby delaying and/or reducing the extent of drug release and hence absorption. On the other hand, FFSAR does not contain isolated silanol groups and instead the largely non-reactive siloxane groups are present on the surface of AR972 which accounts for their hydrophobicity[48,49,51]. It therefore shows lesser hindrance towards desorption and release of the drug as compared to its hydrophilic counterpart. Additionally, since one of the excipient of liquid SNEDDS i.e. SHS15 contains nearly 30% of polyethylene glycol, its adsorption on to the hydrophilic A200 to form FFSA2 would primarily take place via hydrogen bonds between isolated silanol groups and the ether oxygen atoms of the polyethylene glycol, which would ultimately facilitate nucleation and entrapment in the pores[48]. However, the time taken to achieve maximum drug plasma concentration (Tmax) by both S-SNEDDS was 0.5 h. This clearly demonstrates the spontaneity of self-emulsification of the developed formulations despite lower drug release from the solidified SNEDDS. The bioavailability enhancement by LTD loaded S-SNEDDS compared to drug suspension is due to specific combination of selected excipients being meticulously optimized through design of experiment (DOE) approach. The optimized blend of CMC8 and SHS15, upon aqueous dilution, resulted in formation of nanosized globules due to decrease in surface tension by SHS15 that undeniably favors faster emulsification. Also, CMC8 showing high lipid loading capacity and SHS15 causing disruption of intestinal lipid bilayers assists the enhancement of intestinal absorption. The nanosizing being facilitated by gastric motility results in increased surface area leading to increased contact of the nanosized globules with the apical membrane, thereby providing better access to biological membranes and transfer across the intestinal gut wall[57-59]. The mechanism behind the improved drug absorption by these lipidic formulations is attributed to

RSC Advances Accepted Manuscript

the transport of the drug via lymphatic route, bypass of the P-gp mediated GI efflux cytochrome P450 mediated metabolism. The enhanced absorption is being facilitated by the careful selection and combination of oil and surfactants which play vital roles as absorption enhancers and P-glycoprotein inhibitors. Thus, the use of porous carriers in development of solidified SNEDDS can be employed as formulation alternative owing to the advantages they hold while preserving the physiochemical and biopharmaceutical integrity of liquid SNEDDS.

3.6 In silico assessment–GastroPlus™ simulation

The evaluation of the hydrophilic FFSA2 and hydrophobic FFSAR were further made by in silico prediction of their plasma concentration-time profile and simulation of the pharmacokinetic parameters. Such assessments were performed using GastroPlus™ built-in compartmental PK model based on ACAT model to predict the absorption profiles of the developed LTD loaded S-SNEDDS. The input parameters for in silico assessment like pKa (4.33) and solubility (4.59 mg/mL, pH 1.2) were obtained from literature[22] while particle size (Table 1) and PK parameters (Table 2) were determined experimentally. Rest of the parameters like log P (4.54), permeability (7.61 cm/s x 10^{-4}), mean precipitation time (900 s), diffusion coefficient (0.65 cm^2/s x 10^5) and drug particle density (1.2 g/mL) were obtained from ADMET Predictor™ module of GastroPlus™ software. The simulated plasma concentration-time profiles of S-SNEDDS viz. FFSA2 and FFSAR are displayed in Fig. 9 (A, B) and the observed and predicted PK parameters are tabulated in Table 3. The observed and simulated profiles were found to be non superimposable but the prediction accuracy of PK parameters exhibited by fold error (FE) were found to be < 2 signifying good prediction. Comparatively, the systemic availability of the drug was found to be better simulated by FFSAR than FFSA2.

RSC Advances Accepted Manuscript

The regional absorption of LTD when formulated into S-SNEDDS (FFSA2, FFSAR) presented significantly higher absorption from upper small intestine. FFSA2 showed absorption of 86.6% and 13.5% from duodenum and jejunum (1, 2), respectively, with FFSAR showing similar absorption of 86.5% and 13.5%, respectively. The regional absorption profiles of these solidified SNEDDS were found to be identical to the liquid SNEDDS (duodenum, 86.5% and jejunum, 13.5%), but considerably higher absorption from upper GIT when compared to LTD suspension (duodenum, 9.6% and jejunum, 35.3%) (Unpublished data). The similarity in regional absorption between liquid and solid SNEDDS is plausibly the result of lipidic nanoemulsion being ultimately absorbed and the underlying mechanism involved in absorption through various compartments of GIT. Majority of LTD absorption from S-SNEDDS taking place from duodenum is the outcome of faster dissolution of developed S-SNEDDS, as also established by Wu et al., 2015 [60]. The lipidic nanoemulsion is being exposed to local secretions of bile salts and pancreatic juice in duodenum, thereby facilitating lipid digestion and hence absorption. LTD is known to be a substrate of P-gp which is co-localized and works in tandem with CYP3A4, the enzyme mostly responsible for extensive pre-systemic metabolism of the drug. Since high levels of CYP3A levels are reported to be present in duodenal tissue, an increased hindrance towards absorption from conventional dosage forms are expected in such areas. However, interestingly S-SNEDDS have shown maximum absorption through duodenum, clearly indicating inhibition of the metabolism-efflux interplay and thus favouring systemic absorption.

3.7 In vitro-in vivo correlation (IVIVC)

IVIVC was established to obtain relationship between the *in vitro* dissolution and the *in vivo* input rate, described by a mathematical model. The predictability of the IVIVC model was evaluated by internal validation where PK parameters (Cmax and AUC_{0-t}) were predicted

RSC Advances Accepted Manuscript

using the *in vitro* dissolution data based on the correlation model. Deconvolution, which is basically a calculation of cumulative *in vivo* absorption rate from plasma concentration-time data, was performed by various deconvolution models for both FFSA2 and FFSAR formulations (Table 4). Loo-Riegelman method (2-compartment) and 3rd order polynomial function were the best fit deconvolution model and the best fit correlation function, respectively, obtained for both FFSA2 and FFSAR formulations. The best fit model were selected on the basis of high R^2 value and low values of Standard Error of Prediction (SEP), Mean Absolute Error (MAE), and Akaike Information Criterion (AIC). The plots of fraction absolute bioavailability versus fraction vitro release, obtained after deconvolution are displayed in the insets of Fig. 10 (A) for FFSA2 and Fig. 10 (B) for FFSAR. Non-zero y-intercept may represent a lag-time in the systemic absorption. Although the data does not present linear relationship, non-linear function with higher order polynomial equations may be used to describe the data with curvature as also observed by others [61-63]. Thereafter, following convolution in the convolution tab, the observed and predicted plasma concentration-time profiles using the best correlation function was generated for FFSA2 and FFSAR, as depicted in Fig. 10 (A, B). The observed and predicted plots were found to be overlapping indicating good relationship. Higher degree of overlapping, as indicated by high R^2 was observed for hydrophobic FFSAR (0.936) as compared to the hydrophilic FFSA2 (0.910). However, since the immediate-release formulations do not provide longer time-frames to characterize the dissolution or absorption profile, perfect correlation may not be observed[63]. Nevertheless, it still may provide an in vitro profile as a surrogate for in vivo bioavailability.

4.0 Conclusion

RSC Advances Accepted Manuscript

Loratadine (LTD) loaded S-SNEDDS was successfully developed employing hydrophilic and hydrophobic solidifying carriers. The hydrophilic S-SNEDDS (FFSA2) showed excellent and better flowability as compared to the good and passable flowability attained by FFSAR, and also displayed formation of harder compacts revealed by Texture analyzer. An insight into the likely behaviour of these S-SNEDDS upon compaction was also made to investigate their tabletting potential. Both the S-SNEDDS displayed their reconstitution ability to form stable nanoemulsions, evident from the results of percent transmittance, DLS and zeta potential. Though the S-SNEDDS formulated by hydrophilic and hydrophobic Aerosil® resulted in similar drug-release profiles (apparent from acceptable similarity factor), the hydrophobic FFSAR displayed faster release, marked by Q_t (15) probably due to the fact that such carriers have a low specific surface area which improves the dissolution rate as compared to the carriers with high specific surface area. The estimation of contact angle and the drainage time taken by the dry and pre-wetted S-SNEDDS may be advantageous during lubrication and tabletting. The S-SNEDDS attained sufficient wettability manifested by the contact angles lower than 90°, which disregard the use of additional organic solvent to impregnate the solid carrier with the liquid formulation. The solid-state properties of S-SNEDDS characterized by FTIR, PXRD, DSC and TGA-DTA revealed compatibility between the drug and excipients and also confirmed the presence of drug in its solubilized and amorphous state. TEM images confirmed the non-aggregated spherical shape of nanoemulsion globules of S-SNEDDS with size range concordant with the globule sizes analyzed by DLS (less than 50 nm). Also, it displayed the interfacial presence of surfactant over the nanoemulsion globules of redispersed S-SNEDDS. The surface morphology of LTD, A200, AR972 and S-SNEDDS (FFSA2, FFSAR) indicated that the SNEDDS containing LTD in amorphous form was adsorbed on the pores of adsorbent. FFSAR displayed slightly rough-surfaced particles as compared to its smoother counterpart

RSC Advances Accepted Manuscript

(FFSA2) indicating the surface adsorption of SNEDDS apart from being filled into the pores. The post-effect of drug release disclosed presence of numerous pores on the surfaces of dried residues of S-SNEDDS giving a clear picture of the release of the previously adsorbed liquid SNEDDS from these pores. The in vitro data suggesting reduced ability of FFSA2 compared to FFSAR was also reflected by the in vivo studies, affirming the facilitated nucleation and entrapment of drug in the intraparticular pores of FFSA2. The in vivo studies on rats demonstrated high potential of the developed S-SNEDDS viz. FFSA2 and FFSAR to enhance systemic absorption. Additionally, when the plasma-concentration profiles were simulated by GastroPlus^{TM} simulation software, it revealed good prediction accuracy with fold error < 2. Remarkably high absorption of S-SNEDDS from upper small intestine warranted the inhibition of intestinal metabolism and drug efflux. The IVIVC^{TM} module of the software exposed good correlation by the best-fit correlation function obtained upon deconvolution. The observed and the reconstructed plasma concentration profiles were found to be superimposable to each other. The study presented here thus supports the promising development of solidified lipid based SNEDDS, while retaining the physicochemical and biopharmaceutical features of SNEDDS in order to explore their potential as viable dosage forms to facilitate oral absorption of poorly soluble drugs.

Declaration of interest

The authors report no conflicts of interest. The authors alone are responsible for the content and writing of this article.

Acknowledgements

The authors thank Vice-Chancellor, Birla Institute of Technology for providing the facilities. One of the authors (Samridhi) acknowledges Department of Science and Technology, Government of India for the financial support as INSPIRE-JRF (IF120784)

RSC Advances Accepted Manuscript

(Ref. No. DST/INSPIRE fellowship/2012 dated 25 February 2013). Authors are thankful to Sun Pharmaceuticals Pvt. Ltd, Clinical Pharmacology and Pharmacokinetics, Gurgaon, India for providing the necessary facilities with sincere gratitude to Dr. Tausif Monif, Vice President and his research team. Authors acknowledge SICART-CVM, Vallabh Vidyanagar, Gujarat, India and SAIF KOCHI, Cochin, India for extending necessary facilities required for the present work. The constructive comments and suggestions of anonymous reviewers are deeply acknowledged.

References

1. P. Fasinu, V. Pillay, V.M. Ndesendo, L.C. DuToit LC and Y.E. Choonara, *Biopharm Drug Dispos*, 2011, **32**, 185-209.
2. H. Mu, R. Holm and A. Mullertz, *Int J Pharm*, 2013, **453,** 215-224.
3. C.W. Pouton, *Eur J Pharm Sci*, 2000, **11**, S93-S98.
4. C.M.O. Driscoll, *Eur J Pharm Sci*, 2002, **15**, 405-415.
5. S.D. Maio and R.L. Carrier, *J Controlled Release* , 2011, **151**, 110–122
6. X.Q. Chen, O.S. Gudmundsson and M.J. Hageman, *J Med Chem*, 2012, **55**, 7945-7956.
7. C.J.H. Porter, C.W. Pouton, J.F. Cuine and W.N. Charman, *Adv Drug Deliv Rev*, 2008, **60**, 673-691
8. D. Sakloetsakun, S. Dunnhaupt, J. Barthelmes, G. Perera and A.B. Schnurch, *Int J Biol Macromol*, 2013, **61**, 363-372.
9. D.J. Hauss, *Adv Drug Deliv Rev*, 2007, **59**, 667-676.
10. R.N. Gursoy and S. Benita, *Biomed Pharmacotherapy*, 2004, **58**, 173-182.
11. Samridhi, S.K. Singh, P.R.P. Verma and M.N. Ahsan, *Drug Dev Ind Pharm*, 2014, **40,** 1358-1370.

RSC Advances Accepted Manuscript

12. S. Chakraborty, D. Shukla, B. Mishra and S. Singh, *Eur J Pharm Biopharm*, 2009, **73**, 1-15.

13. T. Gershanik and S. Benita, *Eur J Pharm Biopharm*, 2000, **50**, 179-188.

14. K. Kohli, S. Chopra, D. Dhar, S. Arora and R.K. Khar, *Drug Disc Today*, 2010, **15**, 958-965.

15. S. Beg, S.S. Jena, C.N. Patra, M. Rizwan, S. Swain, J. Sruti, M.E.B. Rao and B. Singh, *Coll Surf B: Biointerfaces*, 2013, **101**, 414–13.

16. B. Tang, G. Cheng, J. Gu and J. Xu, *Drug Discov Today*, 2008, **13**, 606-612.

17. C. Dollery (Ed.), *Therapeutic drugs*, Edinburgh: Churchill Livingstone, 1999, Second edition, Volume 2, pp. L96–7.

18. *United States Pharmacopoeia-National Formulary: The official compendia of standards*, Rockville, MD:USP-NF, 2008, pp. 2547–2549.

19. E. Hadzijusufovic, P. Barbara, V.K. Gleixner et al., *Exp Hematol*, 2010, **38**, 896–907.

20. M.V. Soldovieri, F. Miceli and M. Taglialatela, *Chem Res Toxicol*, 2008, **21**, 997–1004.

21. Samridhi, S.K. Singh and P.R.P. Verma, *Drug Dev Ind Pharm*, 2015, DOI: 10.3109/03639045.2015.1052078.

22. URL: www.drugbank.ca/drugs/db00455; Assessed on 05-10-2015.

23. G. Bruni, L. Amici, V. Berbenni, A. Marini and A. Orlandi, *J Thermal Anal Calor*, 2002, **68**, 561-573

24. F. Frizon, J.O. Eloy and C.M. Donaduzzi, *Powder Technol*, 2013, **235**, 532–539.

25. S. Bandari, S. Jadav, B.B. Eedara, R. Dhurke and R. Jukanti, *J Pharm Innov*, 2014, **9**, 141–149.

26. R.M.P. Singh, A. Kumar and K. Pathak, *AAPS Pharm. Sci. Tech,* 2013, **14**, 412-424.

RSC Advances Accepted Manuscript

27. A. Nasca, O. Berkesi, P. Szabo-Revesz and A. Aigner, *J Incl Phenom Macrocycl Chem*, 2009, **64**, 249-254.

28. A. Nacsa, R. Ambrus, O. Berkesi, P. Szabo-Revesz, Z. Aigner, Á. Nacsa, R. Ambrus, O. Berkesi, P. Szabó-Révész and Z. Aigner, *J Pharm and Biomed Anal*, 2008, **48**, 1020–1023.

29. M. El-Hammadi and N. Awad, *AAPS Pharm Sci Tech*, 2012, **13**, 53-58.

30. F. Zeeshan and N.I. Bukhari, *AAPS Pharm Sci Tech*, 2010, **11**, 910-916.

31. P. Patil and A. Paradkar, *AAPS Pharm Sci Tech,* 2006, **7**, E1-E7.

32. C. Li, M.Y. Lee and J.S. Choi, *Pharmazie*, 2010, **65**, 510–514.

33. C. Li, M. Kim and J.S. Choi, *Arch Pharm Res*, 2010, **33**, 1395-1400.

34. M.E. Aulton and T.I. Wells TI (Eds.), *Pharmaceutics: The Science of Dosage Form Design*, Churchill Livingston, London, 2002, Second edition.

35. A. Martin, P. Bustamante, A.H.C. Chun, *Physical Pharmacy*, B.I. Waverly Pvt Ltd, 1994, Fourth edition Indian rep., New Delhi, pp. 457.

36. X. Qi, J. Qin, N. Ma, X. Chou and Z. Wu, *Int J Pharm*, 2014, **472**, 40-47.

37. Samridhi and S.K. Singh, *Research J Pharm and Tech*, 2015, **8**, 452-461.

38. *National Research Council, Guide for care and use of laboratory animals*, The National Academic Press, Washington, DC, 2011, Eighth edition.

39. G. Sharma, S. Beg, K. Thanki, O.P. Katare, S. Jain, K. Kohli and B. Singh, *RSC Adv*, 2015, DOI: 10.1039/C5RA11687B

40. S. Grbic, J.Parojcic, S. Ibric and Z. Djuric, *AAPS Pharm Sci Tech*, 2011, **12**, 165-171.

41. *GastroPlus™: Simulation software for drug discovery and development*, Simulations Plus Inc., Lancaster, CA, USA, 2015, Version 9.0.

42. F. Sun, L. Lee, Z. Zhang, X. Wang, Q.Yu, X.Q. Duan and E.Chan, *Eur J Pharm Sci*, 2015, **77**, 290–302.

RSC Advances Accepted Manuscript

43. *Evonik technical data sheet*-a; URL: https://www.aerosil.com/www2/uploads/productfinder/AEROSIL-200-EN.pdf

44. *Evonik technical data sheet*-b; URL: https://www.aerosil.com/www2/uploads/productfinder/AEROSIL-R-972-Pharma-EN.pdf

45. A.R. Gennaro (Ed), *Remington: The science and practice of pharmacy*, Lippincott Williams and Wilkins, 2000, Twentieth edition, volume 1, pp. 691.

46. M.V. Speybroeck, H.D. Williams, T.H. Nguyen, M.U. Anby, C.J.H. Porter and P. Augustijns, *Mol. Pharmaceutics*, 2012, **9**, 2750−2760

47. A. Krupa, J. Szlek, B.R. Jany and R. Jachowicz, *AAPS PharmSciTech*, 2014, **16**, 623-635.

48. *Basic characteristics of Aerosil® fumed silica*, Technical bulletin fine particles 11, URL: http://www.aerosil.com/sites/lists/IM/Documents/TB-11-Basic-Characteristics-of-AEROSIL-Fumed-Silica-EN.pdf

49. V. Agarwal, A. Siddiqui, H. Ali and S. Nazzal, *Int J Pharm*, 2009, **366**, 44–52.

50. A. Tan, S. Rao and C.A. Prestidge, *Pharm Res*, 2013, **30**, 2993–3017.

51. M.K. Gupta, Y.C. Tseng, D. Goldman and R.H. Bogner, *Pharm Res*, 2002, **19**, 1663-1672.

52. G. Bracco, B. Holst (Eds.), *Science Technologies, Chapter- Contact angle and wetting properties*, Y. Yuan and T.R. Lee, Springer-Verlag Berlin Heidelberg, 2013, First edition, Series volume 51, pp. 15; URL:http://www.springer.com/978-3-642-34242-4

53. R.M.P. Singh, A. Kumar, and K. Pathak, *AAPS PharmSciTech*, 2013, **14**, 412-424.

54. E.P. Lavor, M.V.M. Navarro, F.D. Freire, C.F.S. Aragão, F.N. Raffin, E.G. Barbosa and T.F.A. de Lima e Moura, *J Thermal Anal Calor*, 2014, **115,** 2303.

55. L.A. Ramos and É.T.G. Cavalheiro, *J Thermal Anal Calor*, 2007, **87**, 831–834.

RSC Advances Accepted Manuscript

56. S.K. Singh, P.R.P. Verma, and B. Razdan, *Pharm Dev Tech*, 2010, **15**, 469–483.

57. P. Balakrishnan, B.J. Lee, D.H. Oh, J.O. Kim, M.J. Hong, J.P. Jee, J.A. Kim, B.K. Yoo, J.S. Woo, C.S. Yong and H.G. Choi, *Eur J Pharm Biopharm*, 2009, **72**, 539-545.

58. S. Beg, S.S. Jena, C.N. Patra, M. Rizwan, S. Swain, J. Sruti, M.E.B. Rao and B. Singh, *Coll Surf B: Bioint*, 2013, **101**, 414–13.

59. N. Sermkaew, W. Ketjinda, P. Boonme, N. Padoongsombat and R. Wiwattanapatapee, *Eur J Pharm Sci*, 2013, **50**, 459–466.

60. C. Wu, L. Kou, P. Ma, L. Gao, B. Li, R. Li, C. Luo, J. Shentu, Z. He and J. Sun, *RSC Adv*, 2015, **5**, 19844.

61. T. da S. Honorio, E.C. Pinto, H.V.A. Rocha, V.S.A.D. Esteves, T.C. dos Santos, H.C.R. Castro, C.R. Rodrigues, V.P. de Sousa, L.M. Cabral, *AAPS PharmSciTech*, 2013, **14**, 1244-1253.

62. E. Jantratid, S. Prakongpan, G.L. Amidon and J.B. Dressman, *Clin Pharmacokinet*, 2006, **45**, 385-399.

63. D. Young, J.G. Devane and J. Butler, *In vitro-in vivo correlations*, Plenum Press, New York, 1997.

RSC Advances Accepted Manuscript

List of Figures

Figure 1 Force-displacement curves of (A) FFSA2 and (B) FFSAR: Pre-compaction behavior of granular powder bed (Gr-Co-1 to Gr-Co-4) and compaction behavior of compacts (F-Co-1 to F-Co-4)

Figure 2 Contact angle studies: Wetting behaviour of dry and pre-wet S-SNEDDS

Figure 3 PXRD plots of (A) loratadine (LTD); physical mixtures: PM1 (LTD+CMC8), PM2 (LTD+SHS15); co-melts: CM1 (LTD+CMC8), CM2 (LTD+SHS15) and (B) solidifying agents (A200, AR972) and S-SNEDDS (FFSA2, FFSAR).

Figure 4 DSC thermograms of (A) loratadine (LTD); pure excipients (CMC8, SHS15); physical mixtures: PM1 (LTD+CMC8), PM2 (LTD+SHS15); co-melts: CM1 (LTD+CMC8), CM2 (LTD+SHS15) and (B) Optimized formulation (OF); solidifying agents (A200, AR972) and S-SNEDDS (FFSA2, FFSAR).

Figure 5 Thermoanalytical (A) DTA curves and (B) TGA curves of loratadine (LTD); Aerosil 200 (A200); Aerosil R972 (AR972) and S-SNEDDS (FFSA2, FFSAR).

Figure 6 Transmission Electron Microscopy (TEM) images of S-SNEDDS (A) FFSA2 and (B) FFSAR. Figure (C) displays the closer view of the nanoemulsion globules of FFSAR revealing the structural shape of globules.

Figure 7 Scanning Electron Microscopy (SEM) images: LTD at magnification of x2,500 (A) and at x5,000 (B); solidifying agents at x2,500 viz. A200 (C) and AR972 (D); solid-SNEDD formulations (x2,500) viz. FFSA2 (E) and FFSAR (F); S-SNEDDS before release (x5,000) (G) FFSA2, (H) FFSAR; S-SNEDDS after release (x5,000) (I) FFSA2-D and (J) FFSAR-D.

Figure 8 Pharmacokinetic studies: Plot of observed plasma concentration-time profile of hydrophilic S-SNEDDS (FFSA2) and hydrophobic S-SNEDDS (FFSAR) with clear depiction of the difference in profiles up to 4 h provided in the inset.

Figure 9 Experimental and simulated plasma concentration-time profiles of S-SNEDDS viz. (A) FFSA2 and (B) FFSAR obtained from GastroPlusTM software.

Figure 10 In vitro in vivo correlation of LTD S-SNEDDS (A) FFSA2 and (B) FFSAR: Plots of observed and simulated plasma concentration time profile using dissolution data. Inset: Fraction of in vivo drug release and in vitro drug release.

RSC Advances Accepted Manuscript

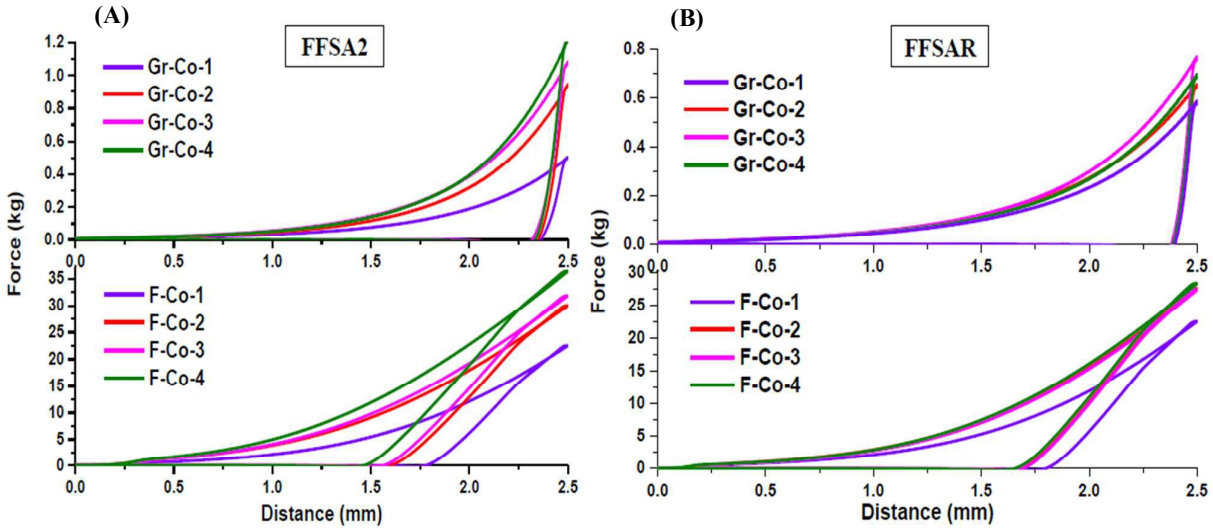

Figure 1

RSC Advances Accepted Manuscript

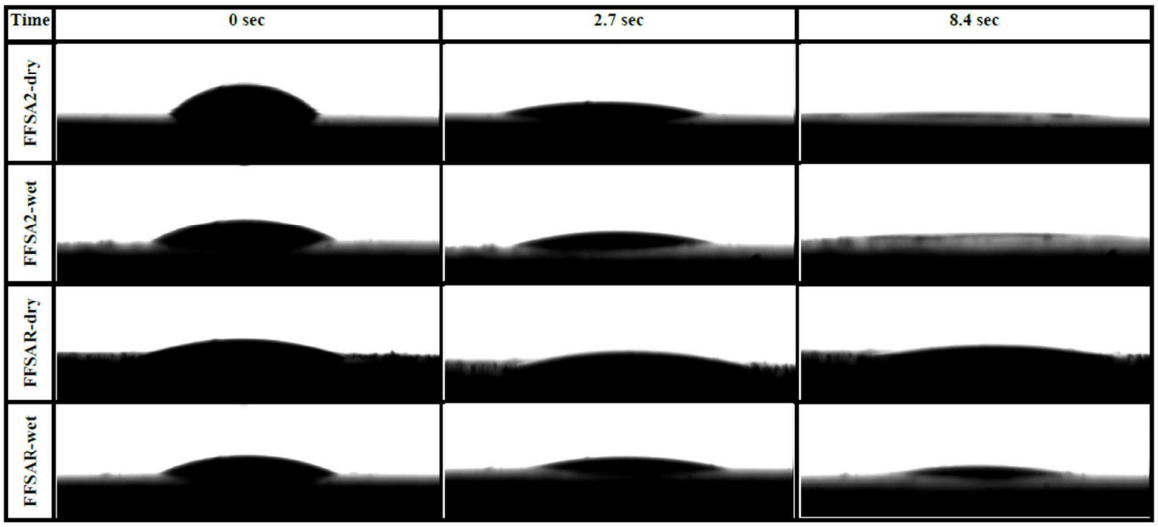

Figure 2

RSC Advances Accepted Manuscript

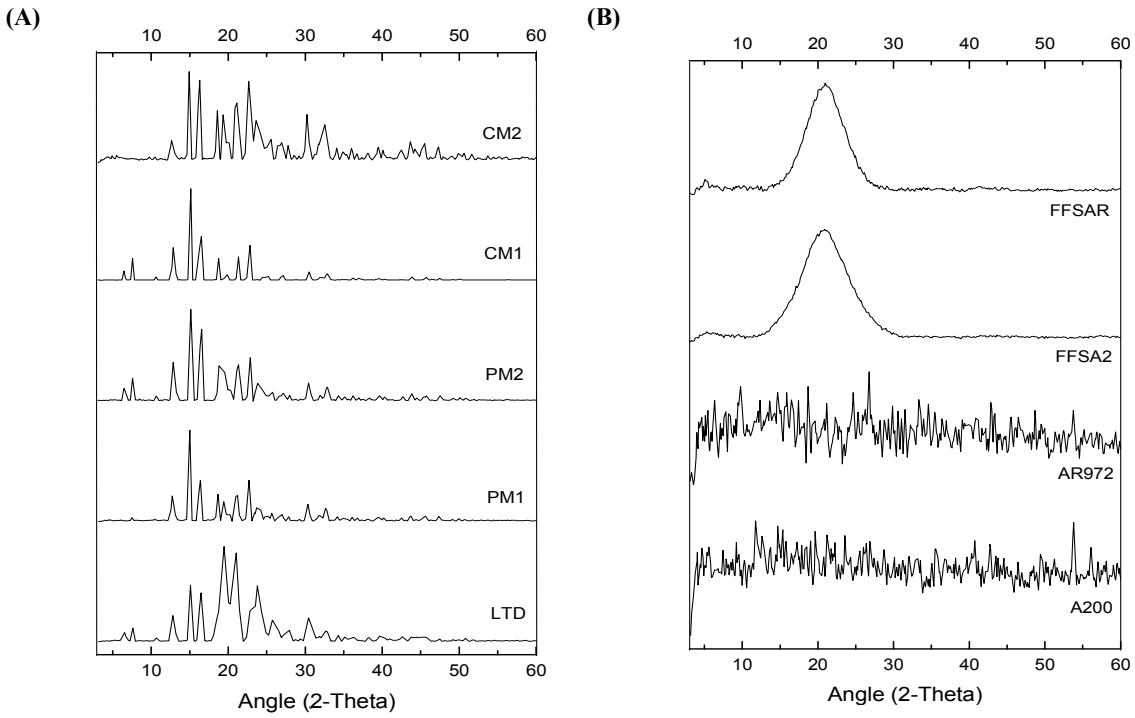

Figure 3

RSC Advances Accepted Manuscript

(A)

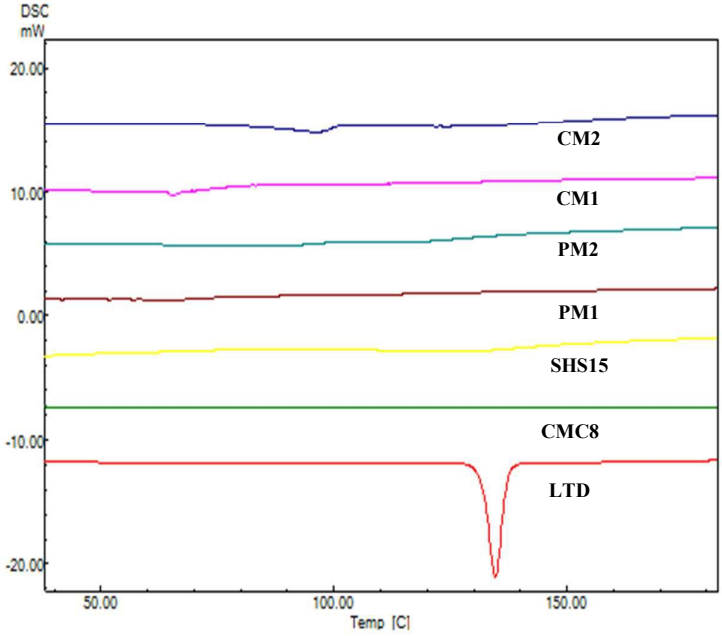

(B)

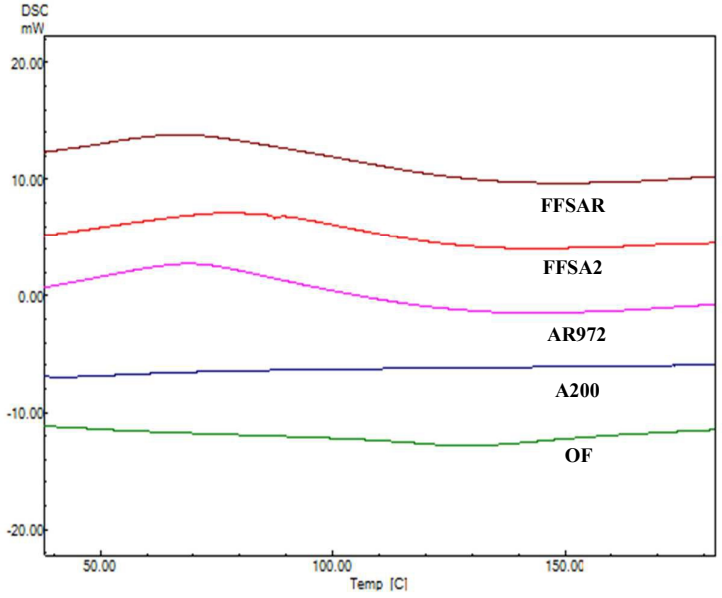

Figure 4

RSC Advances Accepted Manuscript

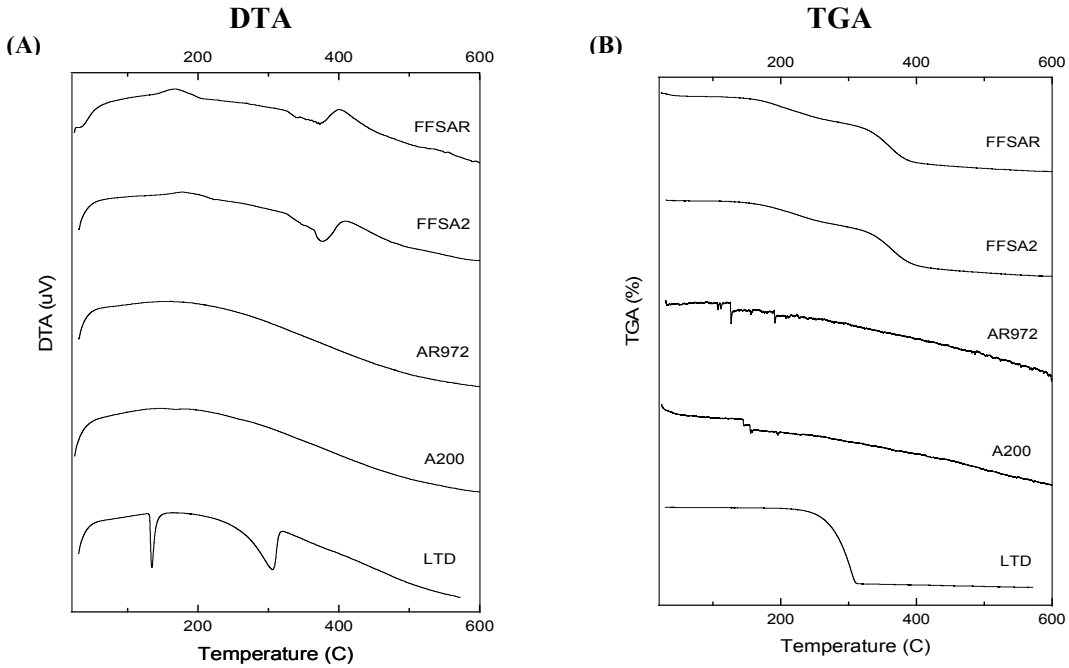

Figure 5

RSC Advances Accepted Manuscript

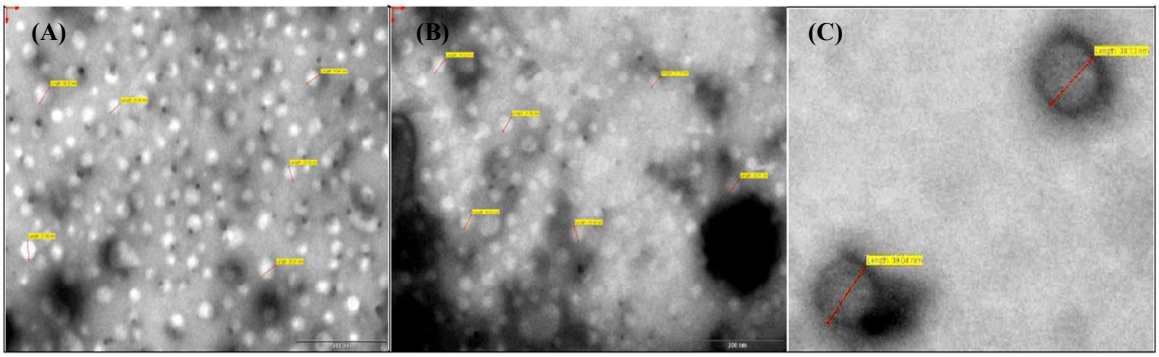

Figure 6

RSC Advances Accepted Manuscript

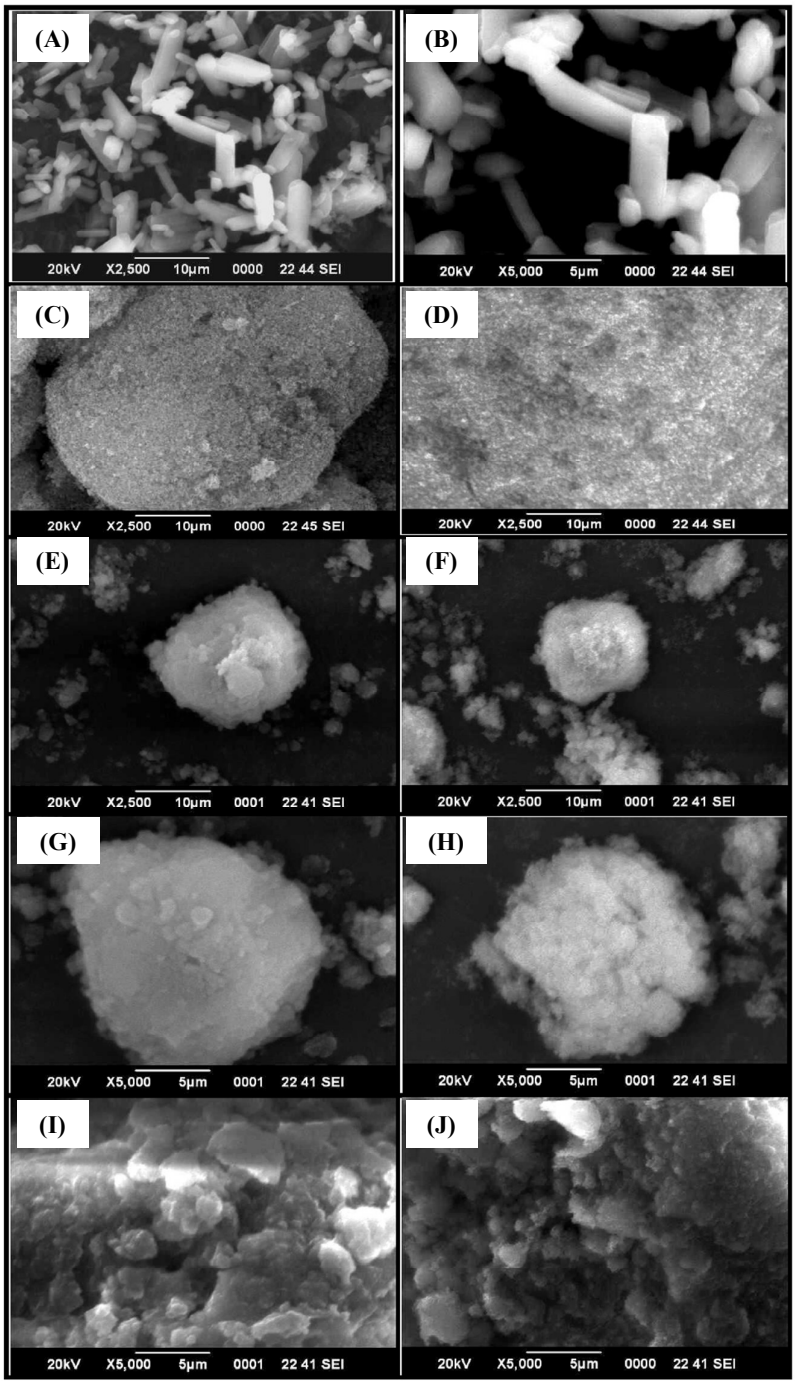

Figure 7

RSC Advances Accepted Manuscript

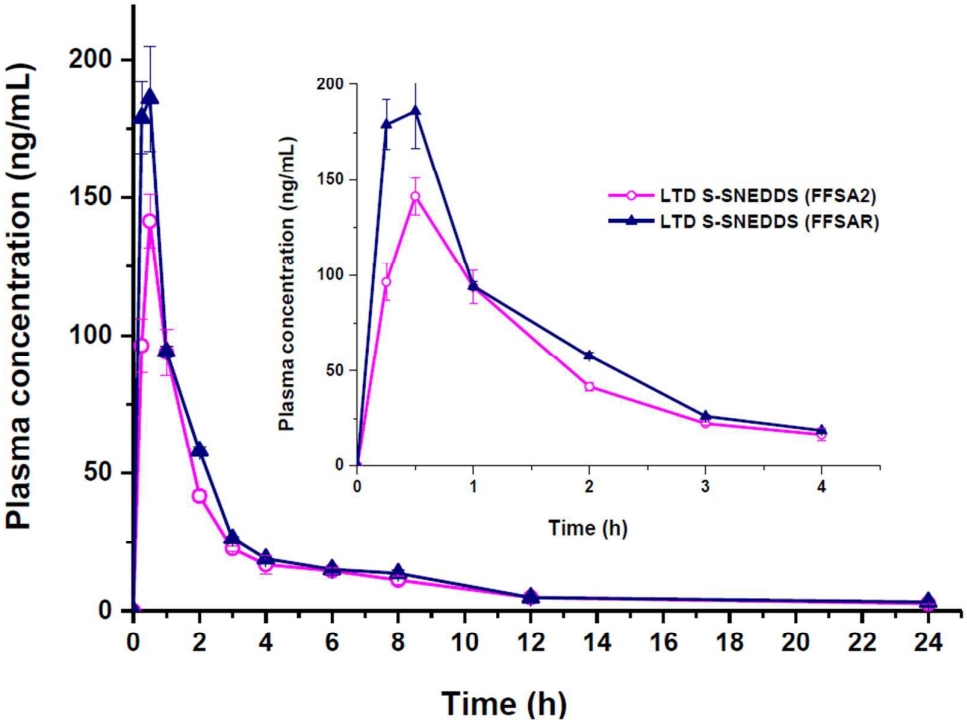

Figure 8

RSC Advances Accepted Manuscript

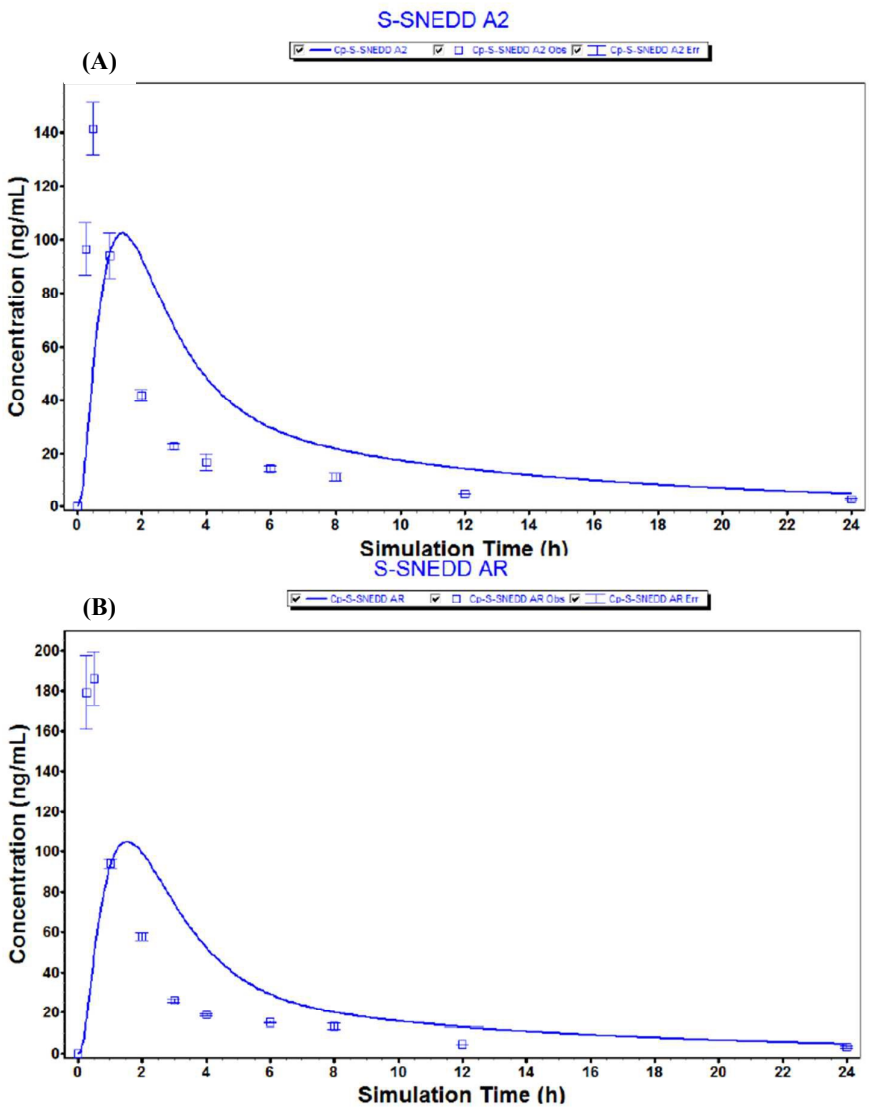

Figure 9

RSC Advances Accepted Manuscript

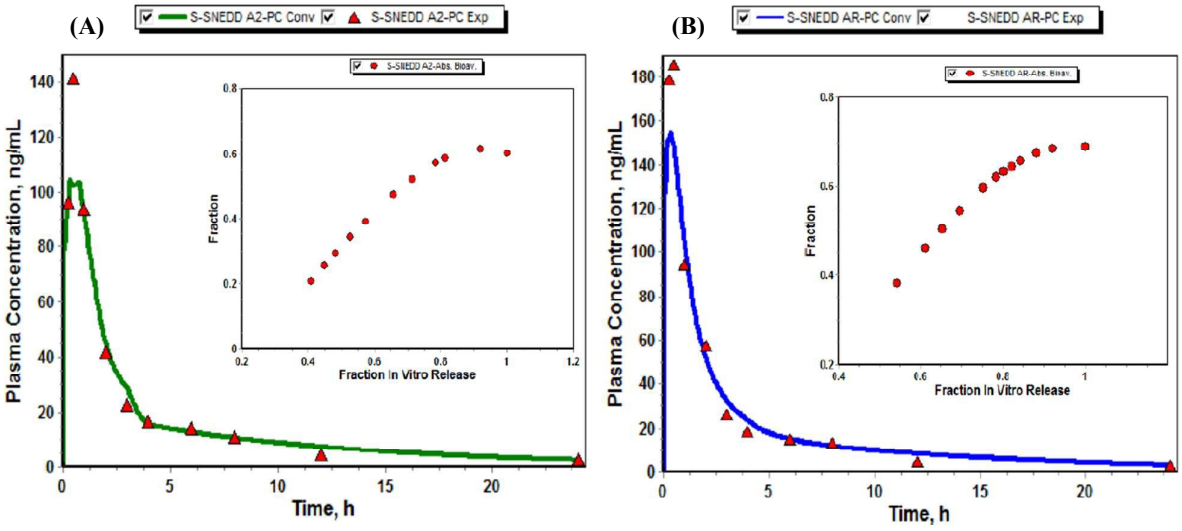

Figure 10

RSC Advances Accepted Manuscript

Table 1

S-SNEDDS: Powder flow properties, physicochemical characterization and dissolution parameters

Bulk properties and flow properties of S-SNEDDS		
Powder Properties	**FFSA2**	**FFSAR**
Weight (gm)	3.26 (0.015)	3.22 (0.025)
Bulk Volume	8.13 (0.115)	8.20 (0.20)
Tapped Volume	6.53 (0.115)	6.43 (0.153)
Bulk Density	0.401 (0.004)	0.393 (0.008)
Tapped Density	0.499 (0.007)	0.501 (0.016)
Hausner's ratio	1.24 (0.004)	1.28 (0.050)
Carr's index (%)	19.67 (0.282)	21.50 (3.037)
Angle of repose (θ)	15.61 (1.816)	20.03 (1.709)
Flow property	Excellent/Fair	Good/Passable

Physicochemical characterization of S-SNEDDS				
	FFSA2		**FFSAR**	
	2h	**24h**	**2h**	**24h**
Per cent Transmittance (400nm)	94.52 (0.15)	92.89 (0.61)	95.94 (0.312)	94.63 (0.62)
Globule size (nm)	27.60 (0.523)	29.2 (0.375)	24.60 (0.566)	26.84 (0.545)
Poly Dispersity Index (PDI)	0.178 (0.022)	0.133 (0.016)	0.171 (0.069)	0.218 (0.033)
Zeta potential (mV)	-24.9 (0.15)	-23.3 (0.495)	-28.2 (0.283)	-27.2 (0.141)
Dissolution parameters				
Drug Loading Efficiency (%)	83.086 (4.781)		83.224 (4.140)	
$Q_{(t)}$ at t = 15 min (%)	48.23 (8.10)		59.33 (4.97)	
Dissolution Efficiency (%)	60.13		66.38	

RSC Advances Accepted Manuscript

Table 2

Pharmacokinetic parameters obtained by non-compartmental and compartmental analysis of LTD loaded S-SNEDDS by PKPlus module of GastroPlus™ software.

Pharmacokinetic Parameters	*FFSA2*				*FFSAR*			
	NC	**1-C**	**2-C**	**3-C**	**NC**	**1-C**	**2-C**	**3-C**
C_{max} (ng/mL)	141.45 (9.72*)				185.99 (18.99*)			
T_{max} (h)	0.5 (0.0*)				0.5 (0.0*)			
AUC_{0-t} (ng-h/mL)	353.00 (0.01*)	407.00 (99.00)	-	-	425.00 (17.53*)	513.00 (107.38)	-	-
$AUC_{0\rightarrow\infty}$ (ng-h/mL)	407.00 (8.80*)	-	-	-	513.00 (24.45*)	-	-	-
AUMC (ng-h^2/mL)	4013.00 (367.72*)	3830.00 (99.00)	-	-	6415.00 (356.57*)	4984.00 (107.38)	-	-
MRT (h)	9.86 (0.81*)	6.27 (84.84)	-	-	12.5 (0.44*)	6.01 (92.03)	-	-
K_{el} (h^{-1})	0.05 (0.02*)	-	-	-	0.036 (0.01*)	-	-	-
$T_{1/2}$ (h)	14.14 (1.33*)	4.35 (84.84)	7.57 (0.00)	265.2	19.25 (0.42*)	4.16 (92.03)	8.164 (0.00)	182.8
CL (L/h)	4.92 (0.61*)	3.28 (51.02)	5.13 (14.18)	1.66 (64.62)	3.51 (1.17*)	2.17 (55.33)	3.74 (17.81)	1.57 (62.65)
Vss (L)	48.49	-	-	-	43.82	-	-	-
Vd (L)	-	20.55 (67.79)	-	-	-	13.03 (73.54)	-	-
Vc (L)	-	-	7.92 (123.77)	6.15 (44.47)	-	-	7.13 (43.7)	6.68 (47.45)
Ka (h^{-1})	-	1.96e+04 (0.00)	2.76 (171.64)	2.21 (48.29)	-	-	7.58 (58.61)	6.66 (60.42)
K10 (h^{-1})	-	0.16 (84.84)	0.65 (124.58)	0.27 (78.44)	-	0.17 (92.03)	0.52 (47.19)	0.24 (78.59)
K12 (h^{-1})	-	-	0.73 (134.14)	0.96 (62.4)	-	-	0.46 (69.89)	0.44 (86.92)
K21 (h^{-1})	-	-	0.21 (61.88)	0.39 (57.32)	-	-	0.17 (71.96)	0.36 (111.41)
K13 (h^{-1})	-	-	-	0.77 (58.18)	-	-	-	0.47 (70.02)
K31 (h^{-1})	-	-	-	0.01 (37.53)	-	-	-	0.01 (51.5)
R^2	-	0.582	0.985	0.985	-	0.568	0.986	0.988
AIC	-	-9.863	-36.059	-38.442	-	-8.069	-30.873	-29.297
SC	-	-8.669	-34.069	-35.657	-	-6.876	-28.883	-26.512

Values marked * represents ±SD; Values in parentheses without * indicate %CV; NC=Non-compartmental; 1-C=One-compartmental; 2-C= Two-compartmental; 3-C= Three-compartmental; AUC=Area under curve; AUMC=Area under moment curve; Cl=Clearance; AIC= Akaike Information Criterion; SC= Schwartz Criterion

RSC Advances Accepted Manuscript

Table 3

Observed and simulated pharmacokinetic parameters of LTD loaded S-SNEDDS obtained by in silico gastrointestinal compartmental simulation by GastroPlus™ software.

Parameter	FFSA2			FFSAR		
	Observed	Simulated	Fold Error (FE)	Observed	Simulated	Fold Error (FE)
C_{max} (ng/mL)	141.45	102.24	1.38	186.00	103.74	1.79
AUC_{0-t} (ng-h/mL)	353.1	584.78	1.66	424.52	584.88	1.38
$AUC_{0-\infty}$ (ng-h/mL)	406.81	637.85	1.57	512.44	640.92	1.25
Fa (%)	-	100.2	-	-	100.00	-
F (%)	-	100.04	-	-	93.18	-

AUC=Area under curve; Fa= Cumulative intestinal absorption; F= Oral bioavailability

RSC Advances Accepted Manuscript

Table 4

Best-fit correlation function, its validation statistics and statistics of reconstructed predicted plasma concentration-time profile of LTD loaded S-SNEDDS (FFSA2 and FFSAR) by various deconvolution models

Methods	Corr. function	Validation statistics						Statistics for reconstructed Cp-time profile			
		C_{max} (ng/mL)			AUC_{0-t} (ng-h/mL)						
		Obs.	Pred.	%Error	Obs.	Pred.	%Error	R^2	SEP	MAE	AIC
S-SNEDDS (FFSA2)											
GastroPlus mechanistic absorption model	Power	141.50	102.1	27.81	345.50	583.50	-68.90	0.356	42.97	30.40	111.10
Numerical deconvolution	Power	141.00	60.00	57.45	345.00	229.00	33.62	0.271	46.28	28.12	112.70
Loo-Riegelman method (2-compartment)	3rd order polynomial	141.00	105.00	25.53	345.00	357.00	-3.478	0.910	12.07	5.245	83.17
S-SNEDDS (FFSAR)											
GastroPlus mechanistic absorption model	Power	186.00	105.00	43.53	420.80	585.60	-39.17	0.220	68.24	41.53	121.3
Numerical deconvolution	2nd order polynomial	186.00	84.00	54.84	421.00	158.00	62.47	0.455	46.83	28.60	113.00
Loo-Riegelman method (2-compartment)	3rd order polynomial	186.00	155.00	16.67	421.00	440.00	-4.513	0.936	14.45	8.799	87.12

AUC= Area under curve; SEP= Standard Error of Prediction; MAE= Mean Absolute Error; AIC= Akaike Information Criterion

RSC Advances Accepted Manuscript

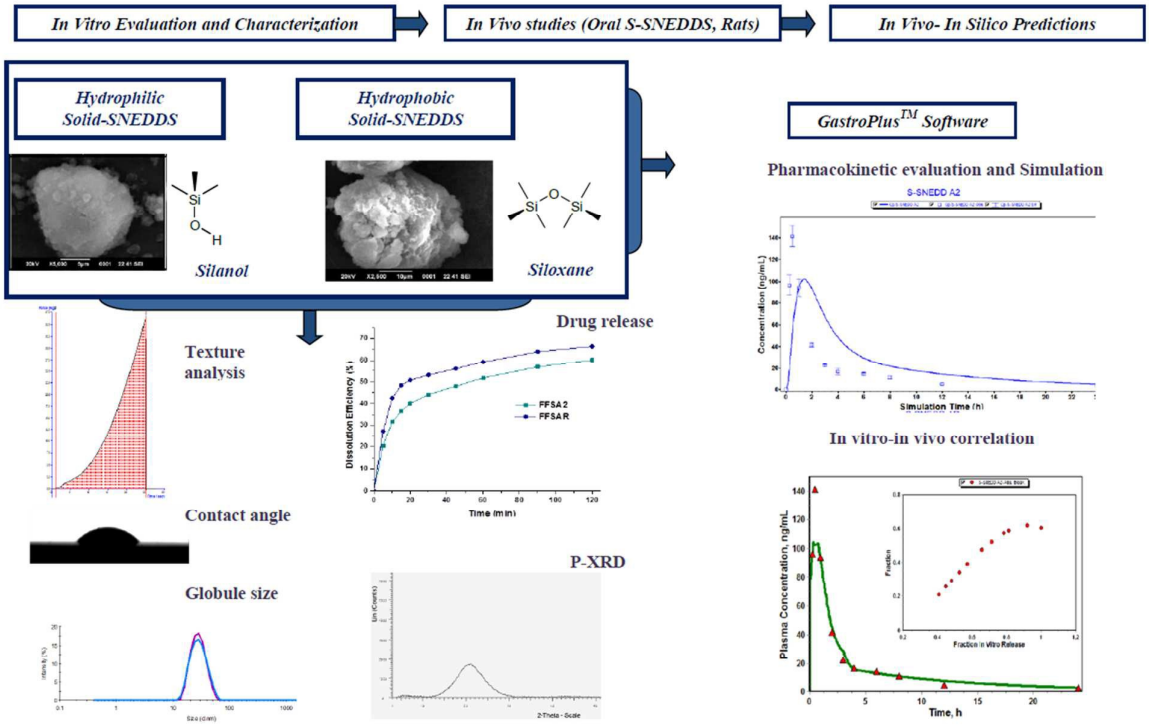

RSC Advances Accepted Manuscript